COLLECTIVE PULSE AMPLIFICATION IN BURST MODE FIBER LASER AMPLIFIERS IN GAIN-MANAGED NONLINEARITY REGIME

A THESIS SUBMITTED TO

THE GRADUATE SCHOOL OF ENGINEERING AND SCIENCE

OF BILKENT UNIVERSITY

IN PARTIAL FULFILLMENT OF THE REQUIREMENTS FOR

THE DEGREE OF

MASTER OF SCIENCE

IN

ELECTRICAL AND ELECTRONICS ENGINEERING

By

Amirhossein Maghsoudi

August 2023

Collective pulse amplification in burst mode fiber laser amplifiers in gain-managed nonlinearity regime
By Amirhossein Maghsoudi
August 2023

We certify that we have read this thesis and that in our opinion it is fully adequate, in scope and in quality, as a thesis for the degree of Master of Science.

Fatih Ömer İlday(Advisor)

Ömer Morgül

Mehmet Emre Taşgın

Approved for the Graduate School of Engineering and Science:

Orhan Arıkan
Director of the Graduate School

ABSTRACT

COLLECTIVE PULSE AMPLIFICATION IN BURST MODE FIBER LASER AMPLIFIERS IN GAIN-MANAGED NONLINEARITY REGIME

Amirhossein Maghsoudi
M.S. in Electrical and Electronics Engineering
Advisor: Fatih Ömer İlday
August 2023

Ultrafast lasers have diverse applications, ranging from optical metrology and spectroscopy to microscopy. Outside of the research laboratory, the most important application continues to be material processing, particularly precision micromachining. In traditional ultrafast processing, high-energy pulses at low repetition rates are used. The recently introduced ablation-cooled regime achieves greater speeds and material removal efficiencies through the use of moderate-energy pulses at much higher repetition rates. However, higher repetition rates also demand short pulses, and higher speeds require higher average powers, such as sub-50 fs pulses at kilowatt average powers. Such parameters are far beyond the current state of the art, but there appears to be no fundamental reason such performance could not be achieved. One common approach to exploit the ablation-cooled regime is to utilized bursts, or groups of pulses. However, such burst-mode amplifiers have resulted in relatively pulse durations to date. This thesis aims to overcome this limitation by implementing burst-mode operation in another recently discovered regime, namely, that of gain-managed nonlinear amplification. In ultrafast laser material processing, sub-50 femtosecond pulse widths and kW average powers are desirable. However, such lasers have yet to be reported in the literature due to the complexity of such systems. For obtaining sub-50 femtosecond pulses, the pulse evolution needs to be well-engineered. Additionally, kW average powers require active cooling systems. A practical method to decrease the average powers in the laser systems yet achieve the same pulse energies is to amplify bursts of pulses instead of a continuous stream of them. These bursts allow the energy to be more confined in time and the average power to be lower. In the no-burst case, various nonlinear pulse amplification regimes aid the design processes and produce high-quality pulses. One such regime is the gain-managed nonlinearity, observed after shifting the gain spectrum towards longer

wavelengths accompanied by nonlinear spectral broadening. This process results in very broad optical spectra and short pulses for the amplified pulses. Obtaining sub-50 fs pulses in the continuous case is often complicated, and the results are hard to reproduce. However, with the gain-managed nonlinearity regime, sub-50 femtosecond pulses can be routinely obtained by correctly choosing the amplifier parameters. Despite that, with the inclusion of bursts, pulse parameters tend to be much worse, mainly due to having non-uniform pulses within a burst. Hence, obtaining sub-50 femtosecond pulses in burst-mode lasers is very challenging, and so far, no such lasers have been reported. Combining this regime with continuously pumped signal burst lasers, we have obtained pulses with 900 nJ energies and sub-50 femtosecond pulse widths with pulse repetition rates as high as 240 MHz and burst repetition rate of 1 MHz. The design process is aided by gaining knowledge regarding the nonlinear amplification process and the gain medium's response time through mathematical modeling and numerical simulations. Burst-mode amplification in the gain-managed nonlinearity regime leads to new physical effects, whereby the amplification of one pulse depends on the other pulses constituting a burst.

Keywords: Ultrafast optics, burst mode lasers, gain-managed nonliearity.

ÖZET

KAZANÇ YÖNETIMLI DOĞRUSAL OLMAYAN ATIM KÜMELERININ FIBER LAZERLERDE KOLEKTIF GÜÇLENDIRILMESI

Amirhossein Maghsoudi
Elektrik ve Elektronik Mühendisliği, Yüksek Lisans
Tez Danışmanı: Fatih Ömer İlday
Ağustos 2023

Ultra hızlı lazerlerin optik metroloji ve spektroskopiden mikroskopiye kadar çeşitli uygulamaları vardır. Araştırma laboratuvarının dışında en önemli uygulama, özellikle hassas mikro işleme olmak üzere malzeme işleme olmaya devam ediyor. Geleneksel ultra hızlı işlemede, düşük tekrarlama oranlarında yüksek enerjili atımlar kullanılır. Yakın zamanda tanıtılan ablasyon soğutmalı rejim, çok daha yüksek tekrarlama oranlarında orta enerjili atımların kullanılması yoluyla daha yüksek hızlara ve malzeme çıkarma verimliliğine ulaşıyor. Bununla birlikte, daha yüksek tekrarlama oranları aynı zamanda kısa atımlar gerektirir ve daha yüksek hızlar, kilowatt ortalama güçlerde 50 fs'nin altındaki atımlar gibi daha yüksek ortalama güçler gerektirir. Bu tür parametreler mevcut tekniğin çok ötesindedir, ancak böyle bir performansın elde edilememesinin temel bir nedeni yok gibi görünmektedir. Ablasyonla soğutulan rejimden yararlanmaya yönelik yaygın bir yaklaşım, kümelerden yani atım gruplarından faydalanmaktır. Bununla birlikte, bu tür çoğuşma modlu amplifikatörler bugüne kadar nispeten atım süreleriyle sonuçlanmıştır. Bu tez, yakın zamanda keşfedilen başka bir rejimde, yani kazanç yönetimli doğrusal olmayan amplifikasyonda küme modu işlemini uygulayarak bu sınırlamanın üstesinden gelmeyi amaçlamaktadır. Ultra hızlı lazer malzeme işlemede, 50 femtosaniyenin altındaki atım genişlikleri ve kW ortalama güçleri arzu edilir. Ancak bu tür lazerler, bu tür sistemlerin karmaşıklığı nedeniyle literatürde henüz rapor edilmemiştir. 50 femtosaniyenin altındaki atımlari elde etmek için atım evriminin iyi tasarlanmış olması gerekir. Ayrıca kW ortalama güçler aktif soğutma sistemleri gerektirir. Lazer sistemlerindeki ortalama güçleri azaltıp aynı atım enerjilerini elde etmenin pratik bir yöntemi, sürekli bir akış yerine atım kümelerini güçlendirmektir. Bu kümeler enerjinin zamanla daha sınırlı

kalmasına ve ortalama gücün daha düşük olmasına olanak tanır. kümenin olmadığı durumda, çeşitli doğrusal olmayan atım amplifikasyon rejimleri tasarım süreçlerine yardımcı olur ve yüksek kaliteli atımlar üretir. Bu rejimlerden biri kazanç yönetimli doğrusal olmayan amplifikasyon rejimidir. Bu rejimde, kazanç spektrumunun doğrusal olmayan spektral genişlemenin eşlik etmesiyle uzun dalga boylarına kaydırılmasından sonra, atımlar için eski rejimlere göre daha uzun spektrumler elde edilir. Bu işlem, güçlendirilmiş atımlar için çok geniş optik spektrumlara ve kısa atımlare neden olur. Sürekli durumda 50 fs'nin altındaki atımların elde edilmesi genellikle karmaşıktır ve sonuçların yeniden üretilmesi zordur. Bununla birlikte, kazanç yönetimli doğrusal olmayan rejim ile amplifikatör parametrelerinin doğru seçilmesiyle rutin olarak 50 femtosaniyenin altındaki atımlar elde edilebilir. Buna rağmen, kümelerin dahil edilmesiyle, atım parametreleri, esas olarak bir çoğuşma içindeki tek biçimli olmayan atımlare sahip olmasından dolayı çok daha kötü olma eğilimindedir. Bu nedenle, küme modlu lazerlerde 50 femtosaniyenin altında atımlar elde etmek çok zordur ve şu ana kadar böyle bir lazer rapor edilmemiştir. Bu rejimi sürekli pompalanan sinyal küme lazerleriyle birleştirerek, 900 nJ enerjili ve 50 femtosaniyenin altındaki atım genişliklerinde, 240 MHz'e kadar yüksek atım tekrarlama oranlarına ve 1 MHz küme tekrarlama oranına sahip atımlar elde ettik. Tasarım süreci, doğrusal olmayan amplifikasyon süreci ve kazanç ortamının tepki süresine ilişkin bilginin matematiksel modelleme ve sayısal simülasyonlar yoluyla kazanılmasıyla desteklenir. Kazanç yönetimli doğrusal olmayan rejimde küme modu amplifikasyonu, yeni fiziksel etkilere yol açar; bu sayede bir atımnin amplifikasyonu, bir küme oluşturan diğer atımlare bağlıdır.

Anahtar sözcükler: Ultrahızlı lazerler, küme modlu lazerler.

Acknowledgement

I would like to thank my advisor Prof. F. Ömer İlday, especially for being patient with me and providing academic and general mentorship, as well as showing how to have a scientific outlook towards various aspects of life. Combining the concepts of nonlinear dynamics with daily life has become a consistent thinking paradigm for me. I would also like to thank my colleagues, starting from Dr. Paul Repgen for his help and discussions on various subjects from laser physics to history and also for being a consistent motivator for post-working hour gatherings, Mesut Laçin for his assistance both inside and outside the laboratory being an older brother for us in the lab, Abdullah Bin Aamer for his long friendship from the first years of undergraduate helping both scientifically and in friendship, Aladin Şura for his blunt and to the point advice in various projects, similarly Buğra Yalçın for his friendship, and Dr. Michaël Barbier and Ghaith Makey for their scientific and friendly advice during my time in UFOLAB as MS student. Last but not least, I would like to thank my family, starting from my mother, Parivash who has sacrificed a lot and has always motivated us to reach great feats in life, my father, Alireza, for his sacrifices and motivation, both as a father and as an engineer, my brother Amirali for being my brother and friend and helping me in life. Only if these few words could be enough to show all the gratitude I sincerely feel because I believe it is a rare privilege to be born into a great family and to get to know nice people in one's adult and professional life.

Contents

List of Figures

List of Tables

Chapter 1

Introduction

Ultrafast fiber lasers, once confined to the research laboratory due to their complexity and high costs, are rapidly evolving into an important tool in cutting-edge industries, used in various fields such as micromachining, in addition to their relatively niche but well-documented applications to biomedical imaging, metrology, and select medical processes [1]. Nevertheless, the most commonly used industrial lasers are, by a large margin, continuous wave (CW), where the light is continuously generated from the laser. However, various processing techniques, including cutting and drilling, with CW lasers lead to extensive thermal damage and, often, residual material formation on the surface because the dominant mechanism is the removal of material by melting, which is blown away with a pressured gas or air [2]. Similarly, ablation with longer pulses in the microsecond (µs) and nanosecond (ns) regimes also suffer from strong thermal effects [2], despite being relatively superior to CW lasers in this regard. It is only the ultrafast lasers, producing femtosecond (fs), or as long as few picosecond (ps) pulses, that result in truly localized removal of material with little or no discernible melting or other thermal effects even in the immediate vicinity of the spot acted upon by the laser beam. The dominant mechanism, in this case, is a highly non-thermal equilibrium process known as ultrafast ablation, whereby material is ejected as a result of a high-speed, instead of melting, only ablate and vaporize the material [3]. Traditionally, ultrafast lasers utilize high-energy pulses such that each pulse

is capable of exceeding the ablation threshold, and, to first approximation, the interaction of each pulse with the target material is independent of the action of any previously delivered pulses. This requires low repetition rates of the pulses, and, indeed, the overwhelming majority of the usage scenarios used kHz repetition rates until recently. In 2016, Ilday et al. showed that high-repetition-rate pulses with individual energies much below the ablation threshold could, nevertheless, collectively ablate a target material, in fact, with much higher efficiency, if they arrived in quick succession (requiring GHz repetition rates) and their total energy was higher than the ablation threshold for a single pulse [4]. In this regime, after a number of sacrificial pulses that merely heat the surface, each of the subsequent pulses ablate the material. The time between the pulses is in the sub-ns range, during which negligible thermal diffusion occurs, the residual heat left at the focal point by each pulse following the ablation it is effectively arrested. Therefore, the dominant mechanism of removal of the heat energy caused by the laser beam becomes the process of ablation, whereby the hot material is rapidly ejected out of the surface, thus momentarily cooling it. It is for this reason that this regime was named as ablation-cooled by its inventors.

The ablation-cooled regime demonstrated order-of-magnitude higher efficiencies while simultaneously reducing the undesired heating of the surrounding region on the target material. However, exploitation of this regime requires a different laser technology designed to produce relatively low-energy pulses but at high repetition rates, typically in the orders of several GHz but as much as tens of GHz, if not more. At such unprecedented repetition rates, the required average pump and signal powers correspond to the order of multi-kW to achieve moderate pulse energies in the range of several µJ. To circumvent this requirement of high average powers, burst-mode lasers were used to achieve the same pulse energies only at a few or tens of W [5]. A burst-mode laser produces a finite number of pulses with a high repetition rate, which is periodically repeated at a much lower burst repetition rate. However, there are specific challenges in designing burst-mode lasers, mainly due to the generation of amplified spontaneous emission (ASE), low pump to signal power conversion efficiency, and uneven gain distribution across the burst, which often result in complicated and cascaded laser designs

[6, 7, 8]. Additionally, like regularly pulsed high-energy lasers, many burst mode lasers similarly tend to have long pulse durations in the range of hundreds of fs [9, 10, 11, 12, 13, 14, 15]. Various specific reasons contribute to the relatively long pulses observed in burst-mode lasers, in addition to the challenges common to ultrafast pulse amplification regardless of uniform or burst-mode operation, such as gain narrowing and accumulation of nonlinear and high-order dispersion-induced chirp. One challenge specific to bursts is the differences in pulse widths among the pulses within the burst, which can stem from many technical reasons, such as uneven gain across the burst, slow electronics, or optical components used to pick the finite group of pulses to define the burst (due to finite rise and fall times), and finally, noise or other unintended modulations over the burst envelope. Another important reason is the complexity of aiming for a specific nonlinear pulse evolution, which is not straightforward to achieve with a burst of pulses since the individual pulses within the burst may experience considerably different nonlinear pulse evolutions. This makes any form of post-compensation of the phase particularly challenging.

In the case of uniform pulse trains, the group of Frank Wise from Cornell University, USA, has recently demonstrated a new amplification regime called the gain-managed nonlinear (GMN) regime, where pulses below 50 fs duration can be obtained [32]. The complex dynamics underlying this regime notwithstanding, the GMN exhibits certain characteristics of dissipative attractor dynamics, which makes it the most plausible candidate for achieving sub-50 fs during burst mode, whereby it is inevitable that the pulses within the burst will exhibit a certain level of inhomogeneity that is simply not typical for uniformed pulsed operation. In the work reported in this thesis, we focussed on the GMN, and demonstrated the first burst-mode GMN amplifier, resulting in pulse energies up to 1 µJ with sub-50 fs pulse durations. These results, in turn, constitute the shortest pulses every generation during burst-mode operation. However, the non-trivial amplification dynamics necessitate a deep understanding of the gain medium's response to the bursts and its interplay with the nonlinear pulse evolution dynamics of the GMN regime, such that the pulses could be compressed to such short durations. Therefore, we first focus on understanding and numerical modeling of burst-mode

and GMN regimes. Next, we present an experimental setup for verification of the insight obtained by the theoretical modeling, and the experimental results are discussed in detail.

From a conceptual point of view, the most significant novelty of burst-mode GMN amplification is that it results in an intricate coupling of the individual nonlinear evolution of the pulses to complex gain dynamics unfolding at a longer different timescale, which, in turn, strongly nonlinearly couples all of the pulses within the burst and from one burst to the others, even though none of the pulses have any direct mechanism of interaction with each other. This coupling represents a new conceptual paradigm that challenges the hitherto established notion that all the major characteristics of amplification of ultrafast pulses can be accomplished by working out the evolution of a single pulse subject to gain dynamics in the steady state. In the burst-mode GMN regime, no such short-cut exists, and the general characteristics of the amplifier pulses are determined *collectively* by all the pulses within the burst. In the last chapter, this topic is further discussed.

Chapter 2

Basics of Ultrafast Pulse Propagation

Light propagation in various media can generally be modeled with Maxwell equations with effective classical terms describing intrinsically quantum mechanical effects such as amplification by stimulated emission or laser noise due to amplified spontaneous emissions. Even though this classical approach is not the most correct model, many physical phenomena of interest are accurately predicted. Pulse propagation is a special form of wave propagation, and with further treatment, an accurate model describing pulse propagation can be obtained. First, this review chapter uses a pulse propagation model from Maxwell equations. Using certain approximations, it is extended to fiber laser amplifiers doped with active media suitable for light amplification. To that end, accurate modeling of the gain media is important to see a range of present effects observed experimentally.

Starting from Maxwell equations, the wave equation in dielectrics can be written as:

$$\nabla^2 \vec{E}(\vec{r},t) - \frac{1}{c_0^2}\frac{\partial^2 \vec{E}(\vec{r},t)}{\partial t^2} = \mu_0 \frac{\partial^2 \vec{P}(\vec{r},t)}{\partial t^2}, \tag{2.1}$$

where $\vec{E}$ is the electric field, and $\vec{P}$ is the polarization response of the medium. The response of the optical media is a function of the incident electric field.

In most media, the linear response is much stronger than the nonlinear one. Therefore, it is a good approximation to write $\vec{P}$ as Taylor expansion with respect to $\vec{E}$:

$$\vec{P} = \epsilon_0(\chi^{(1)}\vec{E} + \chi^{(2)}\vec{E}^2 + \chi^{(3)}\vec{E}^3 + \cdots). \tag{2.2}$$

In equation 2.2, $\epsilon_0\chi^{(1)}\vec{E}$ is the linear response, and higher terms can be grouped as the nonlinear polarization, $\vec{P}_{\text{nonlinear}} = \epsilon_0(\chi^{(2)}\vec{E}^2 + \chi^{(3)}\vec{E}^3 + \cdots)$. Rewriting equation 2.1:

$$\nabla^2\vec{E}(\vec{r},t) - \frac{1}{c_0^2}\frac{\partial^2\vec{E}(\vec{r},t)}{\partial t^2} = \frac{1}{c_0^2}\frac{\partial^2}{\partial t^2}(\chi^{(1)}\vec{E}(\vec{r},t) + \vec{P}_{\text{nonlinear}}(\vec{r},t)). \tag{2.3}$$

By taking the Fourier transform with respect to time, equation 2.3 becomes:

$$\nabla^2\vec{E}(\vec{r},\omega) + \frac{\omega^2}{c_0^2}\vec{E}(\vec{r},\omega) = -\frac{\omega^2}{c_0^2}\chi^{(1)}\vec{E}(\vec{r},\omega) - \mu_0\omega^2\vec{P}_{\text{nonlinear}}(\vec{r},\omega), \tag{2.4}$$

$$\nabla^2\vec{E}(\vec{r},\omega) + \frac{\omega^2}{c_0^2}(1+\chi^{(1)})\vec{E}(\vec{r},\omega) = -\mu_0\omega^2\vec{P}_{\text{nonlinear}}(\vec{r},\omega). \tag{2.5}$$

Noting that many optical media of interest are dispersive ($k = k(\omega)$), and non-magnetic ($\mu_r = 1$), thus using

$$k(\omega) = \frac{\omega}{c_0}n(\omega) = \frac{\omega}{c_0}\sqrt{\epsilon_r\mu_r} = \sqrt{\epsilon_r} = \sqrt{1+\chi^{(1)}}. \tag{2.6}$$

Equation 2.5 can be further simplified as:

$$\nabla^2\vec{E}(\vec{r},\omega) + k^2(\omega)\vec{E}(\vec{r},\omega) = -\mu_0\omega^2\vec{P}_{\text{nonlinear}}(\vec{r},\omega). \tag{2.7}$$

A pulse of light has an oscillating field with an envelope. Initial wave equation 2.1 has a general form for its solutions in the for of:

$$\begin{aligned}\vec{E}(\vec{r},t) &= \vec{A}(\vec{r},t)cos(\omega_0 t - k_0 z)\\ &= \vec{A}(\vec{r},t)(e^{i(\omega_0 t - k_0 z)} + e^{-i(\omega_0 t - k_0 z)})\\ &= \vec{A}(\vec{r},t)e^{i(\omega_0 t - k_0 z)} + c.c.,\end{aligned} \tag{2.8}$$

where $\vec{A}(\vec{r},t)$ is the function that has the pulse envelope information in the frequency domain, and *c.c.* is the abbreviation for the complex conjugate term. Fourier transform of $\vec{E}(\vec{r},t)$ can be written as:

$$\vec{E}(\vec{r},\omega) = \int_{-\infty}^{\infty}\vec{E}(\vec{r},t)e^{i\omega t}dt + c.c. \tag{2.9}$$

Substituting 2.8 in 2.9 we get:

$$\begin{aligned}\vec{E}(\vec{r},\omega) &= e^{ik_0 z}\int_{-\infty}^{\infty}\vec{A}(\vec{r},t)e^{i(\omega-\omega_0)t}dt \\ &= e^{ik_0 z}\vec{A}(\vec{r},\omega-\omega_0). \end{aligned} \tag{2.10}$$

Since polarization response is driven by the input electric field, the nonlinear polarization term can be assumed to have the form:

$$\vec{P}_{\text{nonlinear}}(\vec{r},\omega) = e^{ik_0 z}\vec{P}'_{\text{nonlinear}}(\vec{r},\omega-\omega_0). \tag{2.11}$$

Substituting this and the expression for $\vec{E}(\vec{r},\omega)$ from 2.10, wave equation in the frequency domain shown in 2.7 can be re-written as:

$$\begin{aligned}\nabla^2 e^{ik_0 z}\vec{A} + k^2(\omega)e^{ik_0 z}\vec{A} &= -\mu_0\omega^2\vec{P}'_{\text{nonlinear}} \\ (\frac{\partial^2}{\partial x^2}+\frac{\partial^2}{\partial y^2}+\frac{\partial^2}{\partial z^2})e^{ik_0 z}\vec{A} + k^2(\omega)e^{ik_0 z}\vec{A} &= -\mu_0\omega^2\vec{P}'_{\text{nonlinear}} \\ (\frac{\partial^2}{\partial x^2}+\frac{\partial^2}{\partial y^2}+\frac{\partial^2}{\partial z^2})\vec{A} + 2ik_0\frac{\partial\vec{A}}{\partial z} - k_0^2\vec{A} + k^2(\omega)\vec{A} &= -\mu_0\omega^2\vec{P}'_{\text{nonlinear}} \end{aligned} \tag{2.12}$$

Each material's wave vector $k(\omega)$ is different; however, its variations in most materials are slow around ω_0. Therefore, the dominant terms of $k(\omega)$'s in a Taylor expansion around ω_0 can be used to express it more simply. The first few of these derivative terms are well known with intuitive physical interpretations,

$$k(\omega) = k_0 + k_1(\omega-\omega_0) + \frac{1}{2!}k_2(\omega-\omega_0)^2 + \frac{1}{3!}k_3(\omega-\omega_0)^3 + \cdots \tag{2.13}$$

$$\begin{aligned} k_1 &= \left.\frac{dk}{d\omega}\right|_{\omega_0} = \frac{1}{v_g} && (v_g : \text{group velocity}) \\ k_2 &= \left.\frac{d^2k}{d\omega^2}\right|_{\omega_0} && (k_2 : \text{second order dispersion}) \\ &\vdots \\ k_n &= \left.\frac{d^nk}{d\omega^n}\right|_{\omega_0} && (k_n : \text{n}^{\text{th}} \text{ order dispersion}) \end{aligned}$$

Substituting the first few terms from the Taylor expansion of $k(\omega)$ into equation 2.12 we get:

$$\begin{aligned}&(\frac{\partial^2}{\partial x^2}+\frac{\partial^2}{\partial y^2}+\frac{\partial^2}{\partial z^2}+i2k_0\frac{\partial}{\partial z}-k_0^2)\vec{A}+ \\ &(k_0+k_1(\omega-\omega_0)+\frac{k_2}{2!}(\omega-\omega_0)^2+\cdots)^2\vec{A} = -\mu_0\omega^2\vec{P}'_{\text{nonlinear}}. \end{aligned} \tag{2.14}$$

Using properties of the Fourier transform, equation 2.14 can be written in the time domain as

$$\begin{aligned}&(\frac{\partial^2}{\partial x^2}+\frac{\partial^2}{\partial y^2}+\frac{\partial^2}{\partial z^2}+i2k_0\frac{\partial}{\partial z}-k_0^2)\vec{a}(x,y,z,t)+\\&(k_0+ik_1\frac{\partial}{\partial t}-\frac{k_2}{2!}\frac{\partial^2}{\partial t^2}+i\frac{k_3}{3!}\frac{\partial^3}{\partial \tau^3}\cdots)^2\vec{a}(x,y,z,t)\\&=-\mu_0(\omega_0+i\frac{\partial}{\partial t})^2\vec{P}'_{\text{nonlinear}}(x,y,z,t),\end{aligned}\tag{2.15}$$

where $a(x,y,z,t)$ is the temporal envelope of the pulse, and $\vec{P}'_{\text{nonlinear}}(x,y,z,t)$ is the nonlinear response of the medium in the time domain.

Particular variables and approximation changes can be made to simplify equation 2.15. The first change of variable is to replace the stationary frame of reference t with a non-accelerating one, moving with the pulse envelope group velocity. This retarded time variable τ is defined as $\tau = t - \frac{z}{v_g}$. By using this change of variable and doing some algebra, equation 2.15 becomes:

$$\begin{aligned}(\frac{\partial^2}{\partial x^2}+\frac{\partial^2}{\partial y^2}+\frac{\partial^2}{\partial z^2})\vec{a}+i2k_0(1-\frac{k_1}{k_0}\frac{\partial}{\partial\tau})\frac{\partial\vec{a}}{\partial z}+2k_0D(1+i\frac{k_1}{k_0}\frac{\partial}{\partial\tau})\vec{a}+D^2\vec{a}\\=-\mu_0\omega_0^2(1+\frac{i}{\omega_0}\frac{\partial}{\partial\tau})^2\vec{P}'_{\text{nonlinear}},\end{aligned}\tag{2.16}$$

where D is defined as an operator for all of the higher-order dispersion terms:

$$-\frac{k_2}{2!}\frac{\partial^2}{\partial t^2}+i\frac{k_3}{3!}\frac{\partial^3}{\partial t^3}-\cdots\longrightarrow D=-\frac{k_2}{2!}\frac{\partial^2}{\partial\tau^2}+i\frac{k_3}{3!}\frac{\partial^3}{\partial\tau^3}-\cdots.$$

It should be noted that most such pulses include many optical oscillations under their envelope. Therefore, in equation 2.16, terms concerning the envelope's rate of change in each period of oscillation become very small. Hence:

$$\frac{k_1}{k_0}\frac{\partial\vec{a}}{\partial\tau}\approx 0.$$

Additionally, in waveguides such as optical fibers, the wavelength is much shorter than the beam diameter in the direction of propagation therefore

$$\frac{\partial^2\vec{a}}{\partial z^2}\approx 0.$$

Similar envelope approximation assumptions can be made regarding the nonlinear polarization term, therefore:

$$-\mu_0\omega_0^2(1+\frac{i}{\omega_0}\frac{\partial}{\partial\tau})^2\vec{P}'_{\text{nonlinear}}\approx-\mu_0\omega_0^2\vec{P}'_{\text{nonlinear}}.$$

In terms of dispersion effects, in most optical media, the contribution of 4^{th} order and above terms are very weak in comparison to 1^{st}, 2^{nd}, and 3^{rd} order effects. Hence, from $D^2\vec{a}$ mainly, the impact of the following terms is noticeable:

$$D^2\vec{a} \approx -\frac{k_2}{2!}\frac{\partial^2\vec{a}}{\partial\tau^2} + \frac{k_3}{3!}\frac{\partial^3\vec{a}}{\partial\tau^3}.$$

The last approximation is because, in optical fibers, the beam's transverse distribution variations as it propagates in the fiber are almost zero. This means that if the beam has a specific transverse distribution, it will be maintained throughout its propagation in the fiber. Hence, spatial effects can also be neglected:

$$-\frac{i}{2k_0}(\frac{\partial^2}{\partial x^2} + \frac{\partial^2}{\partial y^2})\vec{a} \approx 0.$$

After considering the above approximations, equation 2.16 can be re-written as:

$$\begin{aligned} i2k_0\frac{\partial\vec{a}}{\partial z} + 2k_0(-\frac{k_2}{2!}\frac{\partial^2\vec{a}}{\partial\tau^2} + i\frac{k_3}{3!}\frac{\partial^3\vec{a}}{\partial\tau^3}) &= -\mu_0\omega_0^2\vec{P'}_{\text{nonlinear}} \\ \frac{\partial\vec{a}}{\partial z} + i\frac{k_2}{2}\frac{\partial^2\vec{a}}{\partial\tau^2} - \frac{k_3}{6}\frac{\partial^3\vec{a}}{\partial\tau^3} &= i\frac{\mu_0\omega_0^2}{2k_0}\vec{P'}_{\text{nonlinear}}. \end{aligned} \tag{2.17}$$

Equation 2.17 is sufficient to model the range of critical optical effects that ultrafast pulses experience in fiber optics. The dominant nonlinear effects can be chosen with their response type and the corresponding parameters to express the $\vec{P'}_{\text{nonlinear}}$ term. The form and values can be taken from the literature or textbooks [16]. For instance, the most dominant nonlinear effect in optical fibers is called the nonlinear Kerr effect, also referred to as self-phase modulation (SPM). In the approximation where nonlinear effects were shown as a Taylor expansion of $\vec{P'}_{\text{nonlinear}}$ concerning the electric field and corresponding electrical susceptibility terms, SPM effects are due to the $\chi^{(3)}\vec{E}^3$ term. The strength of the SPM effect for a given input electric field is determined by the $\chi^{(3)}$ coefficient. The physical mechanism of this effect is creating light at new frequencies resulting from three-wave and four-wave mixing, sum frequency generation, and similar processes. Therefore, only considering the SPM effect, the nonlinear polarization term can be expressed as:

$$i\frac{\mu_0\omega_0^2}{2k_0}\vec{P'}_{\text{nonlinear}} = i\gamma|\vec{a}|^2|\vec{a}|, \tag{2.18}$$

$$\text{where } \gamma = \frac{2\pi n_2}{\lambda_c A_{\text{effective}}}.$$

The γ term above encapsulates all the material parameters in Maxwell equations. The value of n_2, the Kerr coefficient, can be found in many textbooks [17]. λ_c is the carrier wavelength of the pulse (or the central wavelength in mode-locked pulses). $A_{\text{effective}}$ is the effective area in which the light propagates in the medium. Usually, this value corresponds to the mode-field area of the beam in optical fibers.

An equation describing the propagation of ultrafast pulses in optical fibers considering second and third-order dispersion and nonlinear self-phase modulation effects can be written as:

$$\frac{\partial \vec{a}}{\partial z} + i\frac{k_2}{2}\frac{\partial^2 \vec{a}}{\partial \tau^2} - \frac{k_3}{6}\frac{\partial^3 \vec{a}}{\partial \tau^3} = i\gamma|\vec{a}|^2|\vec{a}|. \tag{2.19}$$

The equation 2.19 is known as the nonlinear Schrödinger equation, generalized with the additional of the k_3 term. This model can be further improved to include even higher-order dispersion, stimulated Raman scattering, as well as self-steepening effects [18, 19]. This general nonlinear Schrödinger equation (GNLSE) is defined as:

$$\frac{\partial \vec{a}}{\partial z} - i\sum_{n\geq 2}\frac{i^n k_n}{n!}\frac{\partial^n \vec{a}}{\partial \tau^n} = i\gamma(1 + \frac{i}{\omega_0}\frac{\partial}{\partial \tau})\left[\vec{a}\int_{-\infty}^{\tau} h_R(t')|\vec{a}(z,\tau - t')|^2 dt'\right], \tag{2.20}$$

where $h_R(t)$ is the Raman impulse response in silica fibers with its analytical form taken from the literature with fractional contribution of $f_R = 0.18$ [20, 21].

Including the gain effects requires understanding and modeling the details of the specific gain medium used in pulse amplification. In the next chapter, the characteristics of Yb-doped silica fibers are discussed, a gain model is studied, and the implementation of its numerical solver is shown.

Chapter 3

Gain-Managed Nonlinear Amplification of Pulse Bursts

In ultrashort pulse amplification, depending on the choice of initial parameters, there are various regimes towards which the pulses evolve. These regimes are stable attractors in the nonlinear pulse amplification phase space with a specific basin of attraction. One of these regimes, often seen and utilized in Yb-doped optical fiber amplifiers and oscillators, is the similariton regime. Similariton pulses evolve in a self-similar manner, where they retain their parabolic intensity profiles [31]. However, self-similar propagation involves continuous spectral broadening, which gets disrupted once the bandwidth of the pulse is large enough to experience spectral filtering due to the finite gain bandwidth. A new regime of nonlinear evolution can reach much broader spectra by leveraging the dependency of the spectral profile of the gain to its population inversion level, which varies across the length of the gain medium. This regime is called gain-managed nonlinearity (GMN), where pulses have spectral widths exceeding the net gain wavelengths of the gain medium while maintaining an approximately linear chirp, thus allowing post-compression to pulse widths as short as 40 fs [32]. Given the complete absence of any demonstration of sub-100 fs pulse bursts, this thesis focuses on the adaptation of the GMN regime to burst-mode operation for the first time. However, as will be discussed shortly, this is not straightforward, and it was not

a priori that the GMN regime could be fully attained during the amplification of bursts. The physical reason is that the generation of bursts means that the amplifier is supplied with a signal only a small fraction of the time, which has a significant impact on the inversion level across the gain medium, which, in turn, impacts the gain experienced by the pulses within a burst. We will begin by discussing the general characteristics of how the gain dynamics are affected by the formation of bursts, for which the timescale of the response and response of the gain dynamics is critical. The physics of these phenomena are explored in this chapter, aided by numerical simulations, and verified experimentally. of an experimental setup without bursts are shown. This regime is combined with signal bursts in the next chapter, where certain interesting physics and non-trivial amplification process is observed.

3.1 Modeling Gain Dynamics

Fibers are usually doped with active media, with electronic bandgap structures suitable for light amplification. A common active ion used for this purpose is Yb^{3+} doped in various silica fibers. Light amplification in all active media is done through stimulated emission, where photons with a certain energy or wavelength interact with the active medium, and due to stimulated electron de-excitation, more coherent photons with the same energy are produced. Therefore, this process is intimately dependent on the electronic structure of the active medium. For example, Yb's emission and absorption spectra show the strength of these effects for each wavelength. There can be certain requirements depending on design prerequisites for various applications such as light or pulse amplification or only transmission of short pulses. The required central wavelength of the signal laser light, spectral bandwidth, and amplification per unit length (typically denoted by dB/m) are some of such requirements. Sometimes, the gain bandwidth can be assumed to have a much longer width than the signal. In such cases, knowing the detailed shape of the gain spectrum is not very critical, and either a constant value or a certain functional form can be assumed for the gain spectrum. Lorenzian

and parabolic gain spectral shapes are common in studying or simulating the results of such applications [22]. However, transform-limited pulses with 50 fs pulse widths have spectral bandwidths around 55 nm with 1035 nm central wavelength. An important detail here is the assumption of the pulses being transform-limited. Due to SPM, pulses acquire phase profiles according to their pulse shapes, and if not compensated properly, longer than transform-limited pulses are obtained due to complicated instantaneous phase leading to nonlinear chirp profiles. Therefore, longer spectral widths are required in the presence of some chirp to achieve the same pulse widths. For example, with a central wavelength of 1035 nm, while, normally, a 50 fs pulse requires 55 nm of bandwidth, a pulse with chirp causing pulse duration to be twice the transform-limited one requires approximately a bandwidth of 110 nm. In such cases, gain and pulse bandwidths become comparable, and the exact profile of the gain spectrum becomes important. In this chapter, only realistic gain modeling for Yb is discussed, and the additions are made to the ultrafast pulse propagation equation 2.19.

3.2 Realistic Gain Model

The trivalent ytterbium, Yb^{3+}, can be doped in various host media, which results in unique emission and absorption cross-sections [23, 24]. The critical aspect of Yb^{3+} ion is the existence of two main Stark level manifolds, the ground state, and the excited state [25]. Each manifold has energy sub-levels where electrons transition between them, and these transitions often also involve phonons of specific energy. However, it is impractical to measure the cross-sections between all the pairs of energy levels in Yb^{3+} as well as in many other atoms [25]. Therefore, a common practice is to directly measure the absorption and emission of a medium with many active and host atoms experimentally using a wide-band light source, which yields approximate absorption and emission cross-sections. Such effective cross-section data are helpful in understanding and thus designing laser amplifiers based on various gain media. In Yb-doped optical fibers, in addition to Yb^{3+} and silica, other co-dopants such as germanium, aluminum, and phosphate, are also used to further improve the performance and characteristics of the gain fiber [26].

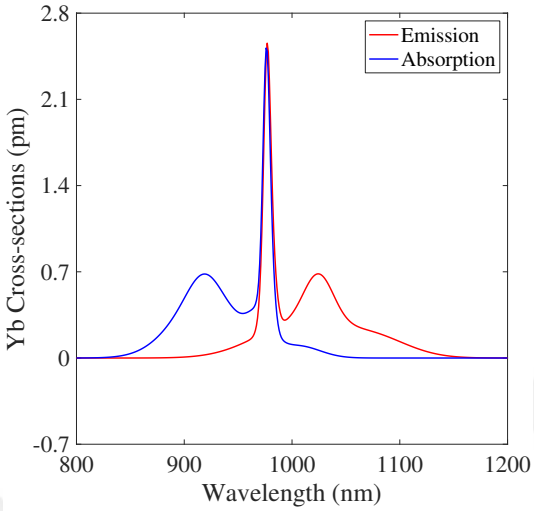

Figure 3.1: Yb's effective emission and absorption cross sections

These added dopants modify the spectral properties of the gain medium; however, the overall qualitative shape of the cross-section spectra is maintained [26]. Even though these data are temperature dependent, noticeable differences in the gain spectra require temperature difference higher than 100s of Kelvin [27]. Additionally, for thermal stability reasons, many laser amplifiers are kept at a constant temperature during their operation at a steady state. Therefore, temperature-induced gain spectrum changes can be omitted under these conditions. For Yb^{3+} doped in germanosilicate glass, measured emission and absorption cross-sections are shown in Figure 3.1 [25].

Our modeling of the gain dynamics is largely based on previous literature work [28, 29, 25], where a two-level system was considered with the following rate equations:

$$\frac{dn_2}{dt} = (R_{12} + W_{12})n_1 - (R_{21} + W_{21} + A_{21})n_2, \tag{3.1}$$

$$\frac{dn_1}{dt} = -(R_{12} + W_{12})n_1 + (R_{21} + W_{21} + A_{21})n_2, \tag{3.2}$$

$$n_1 + n_2 = 1, \tag{3.3}$$

where

n_1 : normalized ground state population, n_2 : normalized excited state population,

R_{12} : pump absorption rate, R_{21} : pump emission rate,

W_{12} : signal absorption rate, W_{21} : signal emission rate,

A_{21} : spontaneous emission rate.

Rates of absorption and emission for photons of the same frequency are proportional to the rate of incoming photons at that frequency and corresponding cross-sections:

$$R_{12} = \frac{\sigma_a(\nu_p)I_p}{h\nu_p}, \qquad R_{21} = \frac{\sigma_e(\nu_p)I_p}{h\nu_p},$$

$$W_{12} = \frac{\sigma_a(\nu_s)I_s}{h\nu_s}, \qquad W_{21} = \frac{\sigma_e(\nu_s)I_s}{h\nu_s}.$$

Here, σ_a and σ_e are the frequency-dependent absorption and emission cross-sections, respectively. For a given photon with frequency ν, division of light intensity with photon energy, $I_p/h\nu$, gives the rate of incoming photons in units of area, or simply photon flux density.

Populations of excited and ground states determine how much gain or loss signal and pump lights will experience in a small fiber segment. A simple model for signal and pump dynamics in the gain fiber can be written as follows:

$$\frac{dP(\nu_s)}{dz} = \eta_s(\sigma_e(\nu_s)n_2 - \sigma_a(\nu_s)n_1)N_{\text{total}}P(\nu_s), \tag{3.4}$$

$$\frac{dP(\nu_p)}{dz} = \eta_p(\sigma_e(\nu_p)n_2 - \sigma_a(\nu_p)n_1)N_{\text{total}}P(\nu_p), \tag{3.5}$$

where η_s and η_p are overlap factors of the signal and pump light with the active ions. N_{total} is the total number of active ions in a small volume of the gain fiber, thus the product of N_{total} with n_2 and n_1 gives the number of excited and ground-state electrons respectively in the same volume of the gain fiber. From equation 3.4, gain coefficient can be defined as:

$$g(z) = \eta_s(\sigma_e(\nu_s)n_2 - \sigma_a(\nu_s)n_1)N_{\text{total}}. \tag{3.6}$$

With this gain model, the GNLSE shown in equation 2.20 can be re-written with the newly added gain parameter as follows:

$$\frac{\partial \vec{a}}{\partial z} - i\sum_{n\geq 2}\frac{i^n k_n}{n!}\frac{\partial^n \vec{a}}{\partial \tau^n} = i\gamma(1+\frac{i}{\omega_0}\frac{\partial}{\partial \tau})\left[\vec{a}\int_{-\infty}^{\tau} h_R(t')|a(z,\vec{\tau}-t')|^2 dt'\right] + g\vec{a}. \tag{3.7}$$

In the literature, several well-known methods are presented for solving the GNLSE, namely, equation 2.20. Some of these methods are split-step Fourier and its many variants and fourth-order Runge–Kutta in the interaction picture (RK4IP) [19, 30]. These methods are based on the so-called interaction picture where, in a finite time window, the state of the pulse is modified explicitly, taking a small forward step in time or space. The modifications are done according to the governing differential equation. Previously used methods for numerically solving GNLSE can still be utilized for a temporally invariant gain term. However, a dynamically evolving gain term means two sets of coupled differential equations, the rate equations determining the gain and GNLSE, must be solved simultaneously. A dynamically changing gain term does not necessarily evolve in time scales relevant to other effects in pulse propagation. For instance, as far as gain dynamics are concerned, in Yb-doped fiber amplifiers, a pulse train with tens of MHz or higher repetition rates can be considered a continuous wave light having a broad coherent spectrum with corresponding powers in each frequency bin. However, ultrafast pulses with high spatiotemporal intensities or bursts of pulses with high total energies can deplete the gain strongly and cause surprisingly quick gain dynamics, leading the amplification of one pulse to depend on the previous ones. Understanding this is key to overcoming the bottleneck of long pulses thus far reported in burst-mode amplifiers. Therefore, in the next section, the response time of the gain medium is studied to understand if gain dynamics

happen in comparable or much longer time scales and whether steady-state gain assumptions are enough in studying or modeling such laser systems.

3.3 Response Time of the Gain Dynamics

When considering the amount of net amplification, thinking of fiber laser amplifiers as a black box with a corresponding amplification parameter is acceptable. However, this simplification ignores many significant effects in amplifying ultrafast pulses and bursts. For instance, the process is non-uniform throughout the fiber, even in the amplification of CW light. Additionally, in pulsed laser amplification, there is a strong spectral dependency, and with pulses undergoing nonlinear spectral broadening, this effect becomes even more pronounced. Similarly, to define a response time for the entire fiber laser amplifier, one must consider gain dynamics not only in a small segment of a fiber but across the entire fiber. First, a small gain fiber segment was studied, and its response time was estimated. Next, these results are generalized to the entire amplifier. The response time for the gain dynamics in a fiber laser amplifier can be defined as the time it takes until gain reaches a fixed ratio, say 90% or 99%, of its steady-state value. Iteratively considering the response time in each small segment, the entire fiber laser amplifier's response time can be approximated. Figure 3.2 shows a piece of gain fiber divided into small segments denoted by short lengths, Δz, with a corresponding response time, T_i. For calculating each T_i, where $i = 1...N$ and $N = L/\Delta z$, where L is the length of the gain medium, it can be assumed that the amplifier is in a steady state, and inside each segment, the signal and pump power change is negligible. Any changes in the input signal and pump powers to the amplifier would translate as sudden changes in power in the subsequent small segments, albeit some experience higher step changes in power than others.

After a step input, the values of I_p and I_s are constant at the pump and signal injection ends of the gain fiber. However, signal and pump intensities are dynamically evolving for subsequent intermediate segments. The initial signal and pump powers that reach any midpoint in the fiber slowly change as the

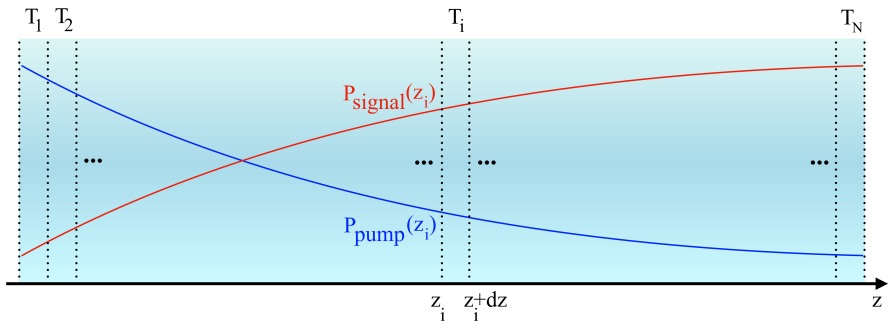

Figure 3.2: A Length of a gain fiber is shown in this figure, which is divided into small dz segments, in which the change of steady state pump and signal powers are negligible. Therefore, power modulations or fluctuations at the input of the gain fiber would propagate sequentially through each segment with its own response time, T_i.

previous segments get pumped, amplifying the signal and reducing the pump further. Thus, the lower and safe limit to the entire amplifier's response time is set by the smallest of the T_i. This is so because the shortest response time means at least some part of the fiber amplifier has not settled to its steady state in response to signal or pump power changes, which puts the most stringent limit on pulse or burst separation. Therefore, we define the full amplifier's response time as:

$$T_{\text{response}} = \min_i T_i. \tag{3.8}$$

If the signal and pump are injected from the same end of the gain fiber, the first small segment will have constant signal and pump powers. Thus, with constant I_p and I_s, the equations for n_1 and n_2, shown in equation 3.1 and 3.2, can be solved analytically to find T_1. The saturation values of n_1 and n_2 in this segment can also be found by finding the equilibrium, or steady state, points from the differential equations. Therefore if

$$\left.\frac{dn_1}{dt}\right|_{n_1^*} = 0, \qquad \left.\frac{dn_2}{dt}\right|_{n_2^*} = 0,$$

the steady state values of n_1 and n_2 are:

$$n_1^* = \frac{B}{A+B}, \qquad n_2^* = 1 - n_1^* = \frac{A}{A+B}, \tag{3.9}$$

where

$$A = R_{12} + W_{12}, \qquad B = R_{21} + W_{21} + A_{21}.$$

As mentioned above, the response time can be defined as when n_1 and n_2 reach, for instance, 1 or 99% of their steady-state values, which can be found by solving the differential equations. For n_1 we have:

$$\begin{aligned} \frac{dn_1}{dt} &= -An_1 + Bn_2 \\ &= -An_1 + B(1 - n_1) \\ &= -(A + B)n_1 + B, \end{aligned} \tag{3.10}$$

and similarly for n_2:

$$\begin{aligned} \frac{dn_2}{dt} &= An_1 - Bn_2 \\ &= A(1 - n_2) - Bn_2 \\ &= -(A + B)n_2 + A. \end{aligned} \tag{3.11}$$

The step-response of n_1 and n_2 would be:

$$n_1(t) = (n_1(0) - n_1^*)e^{-(A+B)t} + n_1^* \tag{3.12}$$

$$n_2(t) = (n_2(0) - n_2^*)e^{-(A+B)t} + n_2^*. \tag{3.13}$$

From equations 3.12 and 3.13, the response time for the segment 1 can be found as:

$$T_1 = \frac{ln(10)}{A + B},$$

or

$$T_1(\nu_s, \nu_p, I_s, I_p) = \frac{ln(10)}{\frac{\sigma_a(\nu_p)I_p}{h\nu_p} + \frac{\sigma_e(\nu_p)I_p}{h\nu_p} + \frac{\sigma_a(\nu_s)I_s}{h\nu_s} + \frac{\sigma_e(\nu_s)I_s}{h\nu_s} + A_{21}}. \tag{3.14}$$

Equation 3.14 shows that response time does not depend on the initial values of n_1 and n_2; rather, it depends on the emission and absorption rates, which in turn depend on signal and pump intensities and frequencies. Suppose we assume that the gain in the subsequent segments of the gain fiber monotonically increases or

decreases. In that case, the overall amplifier's response time will only be decided by the first segment. Because as long as the gain in the first segment has not yet settled, no other subsequent segment will settle either. In that case, the expression for the amplifier's response time can be written as:

$$T_{\text{response}} = T_1(\nu_s, \nu_p, I_s, I_p). \tag{3.15}$$

With further assumptions motivated by experimental considerations, this expression can be simplified. The intensity parameters are approximated by dividing the powers with their respective mode field areas, which ignores the small differences due to the exact spatial profiles of the modes supported by the fiber:

$$I_p(\nu_p, z) \approx \frac{P_p(\nu_p, z)}{A_{\text{pump}}(\nu_p)}, \qquad I_s \approx \frac{P_p(\nu_p, z)}{A_{\text{signal}}(\nu_s)}. \tag{3.16}$$

In optical fibers, more significant differences in mode-field areas stem from the fact that in cladding-pumped amplifiers, pump light is propagated in the cladding and signal light in the core. This corresponds to approximately two orders of magnitude larger mode-field area for the pump than the signal. For simplification purposes, a single value for the mode-field area of the signal and one for the pump can be assumed as effective areas over which the signal and pump light are respectively distributed. Thus, we obtain

$$A_{\text{pump}}(\nu_p) = A_{\text{pump}}, \qquad A_{\text{signal}}(\nu_s) = A_{\text{signal}}. \tag{3.17}$$

Therefore, the expression for amplifier response time can be written as:

$$T_{\text{response}} = T_1(\nu_s, \nu_p, P_s(z=0), P_p(z=0), A_{\text{signal}}, A_{\text{pump}}). \tag{3.18}$$

Mode-locked pulses have broad spectra, and the energy is distributed over many wavelengths. Furthermore, there are often several options for the pump wavelength. In general, the amplifier response time depends on the choice of pump wavelength. In other words:

$$T_{\text{response}} = \min_{\nu_s, \nu_p} T_1(\nu_s, \nu_p, P_s(z=0), P_p(z=0), A_{\text{signal}}, A_{\text{pump}}). \tag{3.19}$$

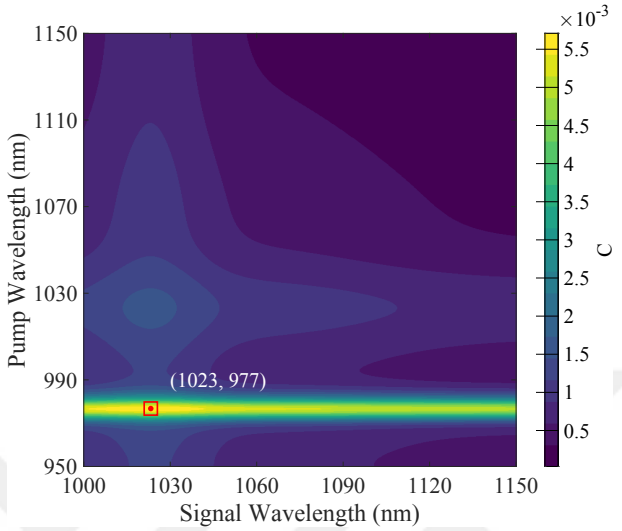

Figure 3.3: Value of cost function C at various signal and pump wavelengths.

From equation 3.14, finding this minimum is the same as finding the greatest value of:

$$C = \frac{\sigma_a(\nu_p)I_p}{h\nu_p} + \frac{\sigma_e(\nu_p)I_p}{h\nu_p} + \frac{\sigma_a(\nu_s)I_s}{h\nu_s} + \frac{\sigma_e(\nu_s)I_s}{h\nu_s}. \tag{3.20}$$

The extreme points of C in equation 3.20 can be found numerically for common signal and pump wavelengths. Figure 3.3. shows the value of C for a range of signal and pump wavelengths. In this range, C has one global maximum at $\lambda_p^* = 977$ (nm) and $\lambda_s^* = 1023$ (nm), corresponding to $\nu_p^* = 307$ (THz) and $\nu_s^* = 294$ (THz) respectively.

Using the optimum signal and pump frequencies, to get a sense of its values, in Figure 3.4, T_{response} was calculated from its analytical expression in equation 3.14, for various pairs of signal and pump step functions. Figure 3.4 has a logarithmic color mapping, showing that depending on the magnitude of the power steps, response time can have orders of magnitude different results. Signal and pump intensities were calculated assuming signal and pump mode-field diameters of 20 and 200 µm, respectively.

With pre-determined signal and pump frequencies, wavelengths, and mode field areas, T_{response} essentially becomes a function of the input signal and pump powers. This simple model can help explain some of the physically observed

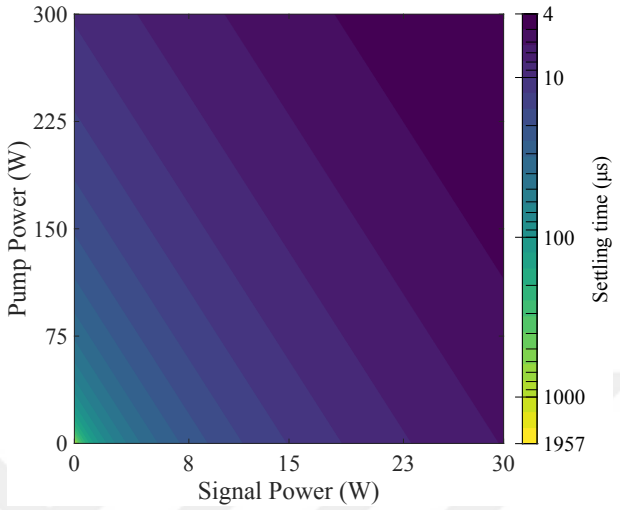

Figure 3.4: The response time of the first segment in a Yb doped gain fiber to a step input of signal and pump with various powers. Signal and pump mode-field diameters were chosen as 20 and 200 µm, respectively.

phenomena in burst mode lasers and guide design considerations. For instance, if the response time of an amplifier is 4 µs for bursts with off-times longer than this value, it would mean that before the arrival of the next burst, the gain medium has a chance to completely recover the energy it has lost during the amplification of the previous burst. However, for burst setups with off-times much shorter than 4 µs, the subsequent bursts arrive before the gain medium has recovered. In cases where burst off-time is much shorter than amplifier response time, the final steady state inversion level, or the gain, in the entire fiber is reached after many bursts. Simulations shown in Figure 3.5 illustrate this effect. To observe the evolution of inversion levels or the gain, only the first segment of the fiber amplifier was simulated, assuming a forward pumping scheme. Simulated bursts have a repetition rate of 500 MHz and an on-time of 500 ns. Four different pairs of signal and pump powers were chosen. The pump was assumed to be continuous with corresponding power, and the signal was delivered in bursts with different on-time average powers. In all the cases, the burst period is much shorter than the amplifier's response time.

In continuously pumped signal burst fiber laser amplifiers, the gain distributed across a single burst is also essential. This is because every signal burst can be

thought of as a step input to the amplifier. Suppose the average power during the on-time of the burst is sufficiently high. In that case, the amplifier will have a reasonably short response time, and gain will start decreasing during the burst's on-time, resulting in unequal burst envelopes, where the leading end of the burst would experience higher gain than the lagging end. This is especially problematic in pulsed burst lasers as pulses under the burst will have different energies and thus different evolution. An important note is that the amplifier response time does not need to be very close to the burst on time for this effect to be seen. The issue is that even if the on-time gain is allowed to change by 5%, that would mean a burst envelope with a 5% power difference between the leading and the lagging edge. In order to avoid seeing this effect, the response time after a signal burst step needs to be sufficiently long that gain has barely any chance of settling during the on-time of the burst. In Figure 3.5, the sub-figures on the right column have no unequal gain effects during the burst on-times, but for the sub-figures on the left column, 5 to 10% variations in the gain are seen during the on-time of the burst, hence the saw-tooth like gain evolution.

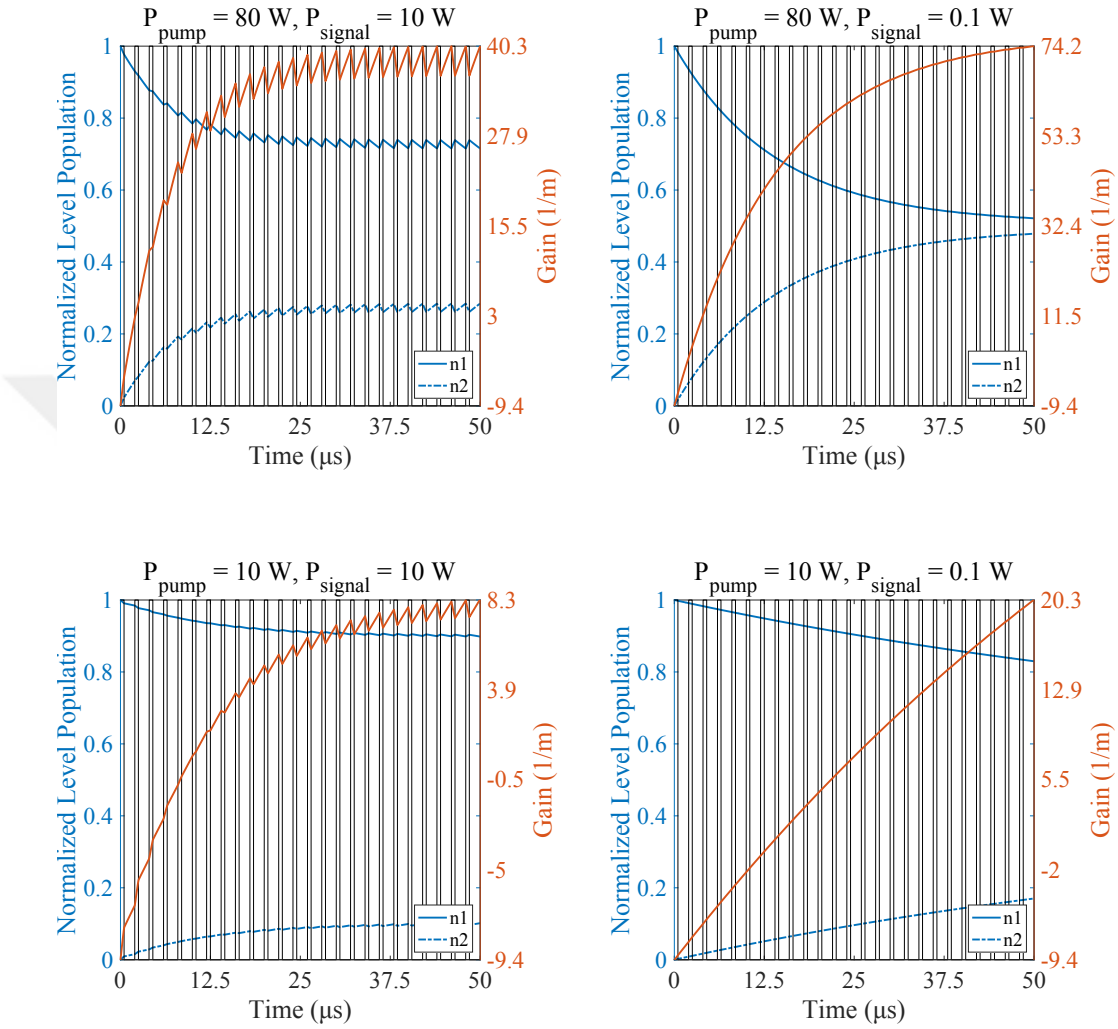

Figure 3.5: Transient response of normalized population levels and gain to step changes of signal and pump power at the beginning of the gain fiber. Simulations take into account typical 25µm LMA gain fiber parameters.

With the insight obtained from this discussion, the steady state gain can be assumed to simplify the simulations if the power values are correctly chosen for numerically simulating a realistic gain combined with the GNLSE equation. The following section discusses the implementation of the numerical algorithm for solving GNLSE with realistic, steady-state gain.

3.4 Numerical Simulations with Realistic Gain

To numerically solve:

$$\frac{\partial \vec{a}}{\partial z} - i\sum_{n\geq 2}\frac{i^n k_n}{n!}\frac{\partial^n \vec{a}}{\partial \tau^n} = i\gamma(1+\frac{i}{\omega_0}\frac{\partial}{\partial \tau})\left[\vec{a}\int_{-\infty}^{\tau} h_R(t')|a(z,\vec{\tau}-t')|^2 dt'\right] + g\vec{a}, \quad (3.21)$$

the following two operators were defined:

$$\hat{D} = -g - i\sum_{n\geq 2}\frac{i^n k_n}{n!}\frac{\partial^n}{\partial \tau^n},$$
$$\hat{N} = i\gamma(1+\frac{i}{\omega_0}\frac{\partial}{\partial \tau})\left[\int_{-\infty}^{\tau} h_R(t')|a(z,\vec{\tau}-t')|^2 dt'\right]. \quad (3.22)$$

In the steady state, the g term is defined as:

$$g(z) = \eta_s(\sigma_e(\nu_s)n_2^* - \sigma_a(\nu_s)n_1^*)N_{\text{total}}, \quad (3.23)$$

where the steady state normalized level populations were found in the previous section in equation 3.9. Pump power is provided as input for calculating these steady-state values, but signal power is calculated by multiplying the energy in each frequency bin with the pulse repetition rate. Therefore, at each small Δz segment of the fiber, for a given pulse power spectral density and pump power, there is a unique gain value g. Therefore, in the operator $\hat{D}$, coefficient g is a constant. This allows us to perform the gain calculations in this linear operator. Therefore, it is possible to implement the RK4IP algorithm with this gain model and use its high accuracy [30].

Field intensities inside the fiber were calculated by dividing the power with the mode-filed area, in short MFA, of the light at each frequency. Therefore:

$$|\vec{a}(\nu)|^2 = \frac{\text{power}(\nu)}{\text{MFA}(\nu)}, \quad (3.24)$$

with the units: $[\vec{a}] = \sqrt{\frac{W}{m^2}}$, [Power] $= W$, and [MFA] $= m^2$. Assuming a step-index fiber, the MFA was calculated from mode-field diameter, or MFD, using Marcuse's equation, which depends on fiber's core diameter, D_{core}, and waveguide number, V. Thus:

$$\text{MFD} = D_{core}\cdot(0.65 + \frac{1.619}{V_0^1.5} + \frac{2.879}{V_0^6}). \quad (3.25)$$

Waveguide number V is a function of wavelength, core diameter, and numerical aperture (NA). In double-clad fibers, signal light in the core and pump light in the cladding have their respective NA values. The expression for V is:

$$V = \frac{2\pi}{\lambda} \cdot \frac{D_{\text{core}}}{2} \cdot \text{NA}. \tag{3.26}$$

Overall, a computationally low-cost but capable numerical model was developed for simulating the gain dynamics of nonlinear propagation of ultrafast pulses in optical fibers.

3.5 Dynamics of the Gain-Managed Nonlinearity Regime

Similariton evolution is only seen in normal dispersion media with positively chirped final pulses [31]. This regime has a large basin of attraction, and for a large set of initial conditions, pulses still evolve towards this regime [33]. The distinct feature of the self-similar amplification is the exponential scaling of its parabolic pulse amplitude and temporal widths [31]. Yb doped gain fiber-based oscillators and amplifiers are common hosts for this regime due to silica fibers having normal dispersion around Yb's emission wavelengths of 1.050 µm [34]. Self-similarly evolving pulses are subject to spectral broadening [35]. This process can continue as long as the bandwidth of the gain spectrum is larger than the optical spectrum of the pulses. However, when these spectra are comparable, self-similar evolution is hampered. The evolution trajectory deviates from this attractor, and this is assumed to be the limit of similariton evolution in many rare-earth doped gain fibers [36, 37]. However, it was recently shown that if pulses are allowed to propagate beyond this gain-narrowing limit, the pulse evolution enters another regime named gain-managed nonlinearity for certain initial conditions. In this regime, pulses accumulate large degrees of nonlinear phase around 200π, yet they still have somewhat linear chirps and are compressible [32]. In similariton evolution, all spectral broadening happens in the wavelength range for which the gain is positive, and the gain spectrum has a parabola-like single

positive peak. In contrast, pulses in the GMN regime experience further spectral broadening, and their spectra go beyond the positive gain regions. This means that after some point in the gain fiber, some portion of the optical spectrum of the pulses experience absorption while others experience amplification. Due to this effect, the final dispersed pulse shape has an asymmetric envelope. Thanks to approximately linear chirps, GMN pulses with sub-50 fs duration were reported in the literature [38, 32, 39, 40]. This regime has been implemented with single mode and LMA fibers, Yb and Er-doped gain media, amplifiers, and oscillators.

The key to obtaining this regime is considerable SPM-induced spectral broadening at the beginning of the gain fiber. In the remainder of the gain fiber, the optical spectrum is further shaped to its final form with gain filtering and selective amplification. Early fast spectral broadening is necessary to amplify enough photons at longer wavelengths. Modification of the gain spectrum is also needed to deform the spectrum and have spectrally asymmetric amplification. Strong SPM broadening at the beginning of the fiber is obtained by having a sufficiently high initial peak power for the seed light and sufficiently high unsaturated or small-signal gain at the beginning of the gain fiber. In Yb amplifiers, the spectral shifting of the gain towards longer wavelengths, often called red-shifting, is possible by having lower inversion levels. Therefore, judiciously chosen pump power and high-intensity signal at the beginning cause just enough pump depletion such that the gain spectrum in the remainder of the gain fiber has the desired shape, absorbing shorter wavelengths and amplifying long ones. An important note here is that, in Yb amplifiers, red-shifting of the gain mainly refers to the gain in longer wavelengths being comparable to that of the shorter ones. With the gain and simulation model discussed previously, the process of red-shifting of the gain is shown in Figure 3.6

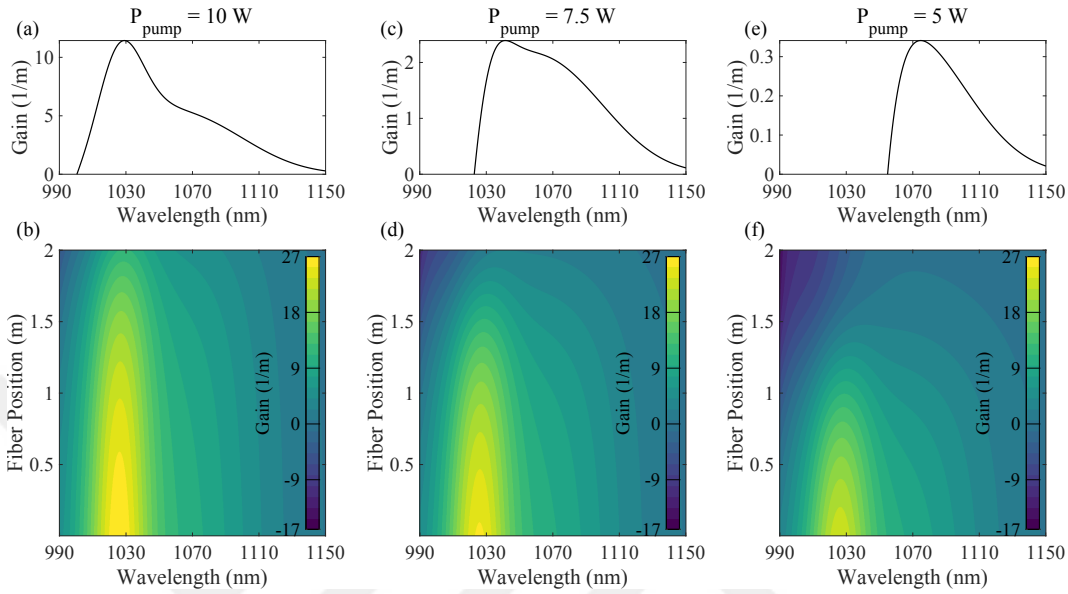

Figure 3.6: Gain red-shifting is shown via simulations. In all the figures, the signal power was 0, and only by changing the pump power different inversion and gain profiles were obtained. Realistic physical values for the gain fiber were used, assuming a 2-meter-long gain fiber. (a) and (b) are with 10 W pump powers, where (b) shows the positive gain spectrum at the end of the gain fiber, similarly for (c-d) 7.5 W and (e-f) 5 W pump powers, respectively. ASE effects were ignored.

3.6 Numerical Simulations of GMN Regime

For designing an amplifier working in the GMN regime, numerical simulations provide invaluable insight into the choice of parameters, which, it must be noted, is less forgiving than similaritons. In other words, although the GMN regime exhibits features of a dynamic attractor, its basin of attraction is significantly narrower than for similaritons. For instance, the simulations can clarify for which parameter values the pulses successfully evolve towards the GMN regime with a fully coherent spectrum and approximately linear chirp. In our simulations, key parameters such as core and cladding NA, Yb^{3+} concentration, dispersion, and nonlinearity coefficients were taken from product datasheets or close approximations from literature. The noise was chosen to be zero for the sake of simplicity. Table 3.1 lists these parameters.

Table 3.1: **Constant Parameters Used in the Simulations**

Parameter	Unit	Value
Fiber Length	m	2
Core NA	-	0.062
Cladding NA	-	0.48
Yb^{3+} doping concentration	ions/nm^3	0.1
Group velocity dispersion (GVD)	fs^2/mm	18
Third order dispersion (TOD)	fs^3/mm	42
Kerr coefficient (n_2)	cm^2/W	2.3×10^{-16}
Raman response contribution (f_R)	-	0.18
Added noise	photons/frequency	0

The next step was optimizing the initial pulse parameters and finding the optimum values for which broad optical pulse spectra in the GMN regime are obtained. Figure 3.7 shows these optimization simulations. In each case, around a particular set of values, one of the four variables of pulse energy, central wavelength, spectral width, and pulse duration was swept across a reasonable range of values, and the remaining ones were kept constant. All of these simulations hint at the critical fact, namely, that the initial peak power of the pulse determines whether the pulse will evolve toward the GMN regime. For example, if the initial peak intensity is too low, SPM broadening will fall short of supporting spectral broadening to be amplified by the gain response that shifts to longer wavelengths further along the amplifier, where the inversion level is decreasing, thus failing to reach the GMN regime.

To see the importance of the initial peak intensity of the pulse, Figure 3.8 shows a set of simulations where, in each case, every parameter was kept constant except the amount of added positive chirp, resulting in pules of varying peak intensities. This figure shows that initial peak intensity determines whether the pules will evolve to similariton, or GMN regimes, or be somewhere between, which usually means incompressible nonlinearly chirped pulses.

The influence of some of the critical parameters on the seed's peak intensity can be summarized as:

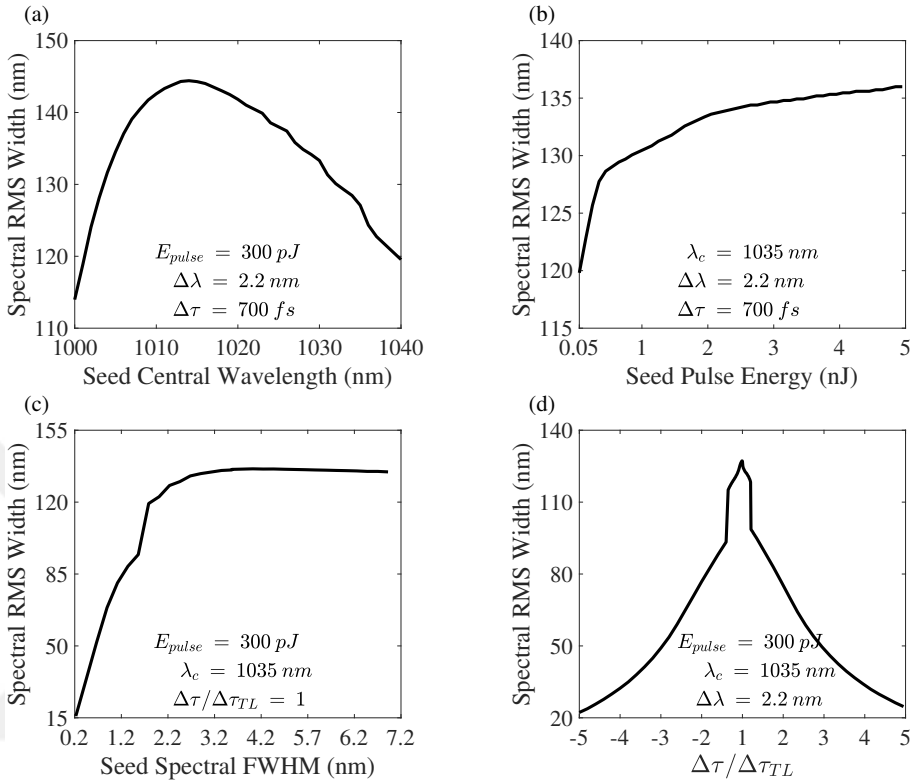

Figure 3.7: Parameter optimization simulations were performed around common literature values to reach the GMN regime in LMA fibers and find the most optimum values. In (a), only the central wavelength of the seed, (b) pulse energy, (c) spectral width, and (d) chirp values were swept, keeping the other seed parameters constant, which are written inside each figure.

- Unlike similariton evolution, rather than the seed pulse energy, the most relevant factor is the initial peak intensity. It must be high enough for rapid SPM-induced broadening to evolve the pulses toward the GMN regime.

- A given peak power can be achieved with lower energies for shorter pulses, but if the pulse duration is too short, dispersion will broaden the pulses, thus lowering the peak power too quickly. Optical pulse duration appears to be in the range of 1 ps for typical fiber parameters.

- The peak power, thus seed energy must not be too high either because it can result in premature onset of stimulated Raman scattering (SRS), which must kick in only after the spectrum has sufficiently broadened towards longer wavelength.

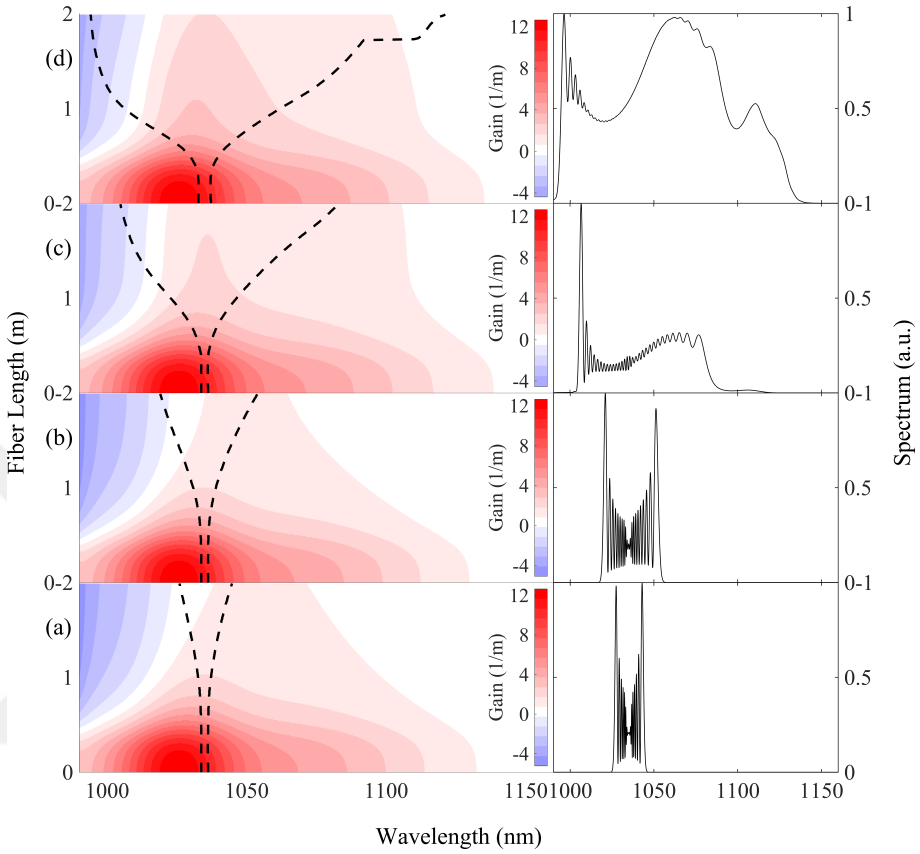

Figure 3.8: This figure numerically shows the transition from similariton to the GMN regime by only modifying the seed pulse's peak power by adding various amounts of positive chirp. In (a), the pulse is in the similariton regime, and its spectrum is confined to positive gain regions. (b) is the limit of this regime in Yb doped gain media as the finite gain spectrum is limiting spectral broadening. In (c), the pulse spectrum experiences strong gain shaping. (d) is beyond gain shaping entering the GMN regime.

- The amount of chirp on the initial pulse again directly determines the seed's peak intensity and has similar effects as the above two parameters, also limited by SRS.

- The central wavelength of the seed is critical because it determines the gain that the pulse will experience early in the gain fiber. If this gain is low, pulses do not reach and maintain sufficient peak powers during propagation. Nevertheless, the amplification process has to slow down eventually, and pump depletion must allow for broadening and red-shifting of the gain profile; otherwise, the necessary gain red-shifting will not occur.

- The relatively narrow basin of attraction of the GMN regime arises due to these multiple considerations. Our impression is that the GMN regime is more similar to the amplifier soliton dynamics for the anomalous dispersion regime than the similariton regime in terms of accommodating different initial parameters.

The interval of peak power for which pulses reach the GMN regime can be thought of as the basin of attraction of the GMN regime. The size of this basin is a function of many parameters, but a general statement deduced from the simulations can be approximately stated as:

$$\begin{aligned} &\text{basin of attraction of GMN} = \\ &f(\text{seed peak intensity}, \text{small-signal gain}), \end{aligned} \tag{3.27}$$

where the seed peak intensity and small signal gain of the amplifier, in turn, are functions of:

$$\text{seed peak intensity} = g_1(E_{\text{pulse}}, \Delta\tau, \text{MFA}_{\text{signal}}), \tag{3.28}$$

$$\text{small-signal gain} = g_2(\lambda_c, P_{\text{signal}}\text{MFA}_{\text{pump}}). \tag{3.29}$$

This understanding is motivated by the numerical simulations. However, further development of this could lead to gaining more insight into the details of this regime.

3.7 Experimental Results

The laser setup shown in Figure 3.9 was developed in the laboratory to implement GMN amplification. It consists of a Mamyshev oscillator mode-locked at various harmonics of its fundamental repetition rates. However, only the fundamental harmonic at 15 MHz was used for the experiments reported in this chapter to decrease the average power requirements for reaching high pulse energies. After coupling the free-space seed light from the oscillator to the fiber line, the light was first amplified in a pre-amplifier stage to increase the pulse energy entering

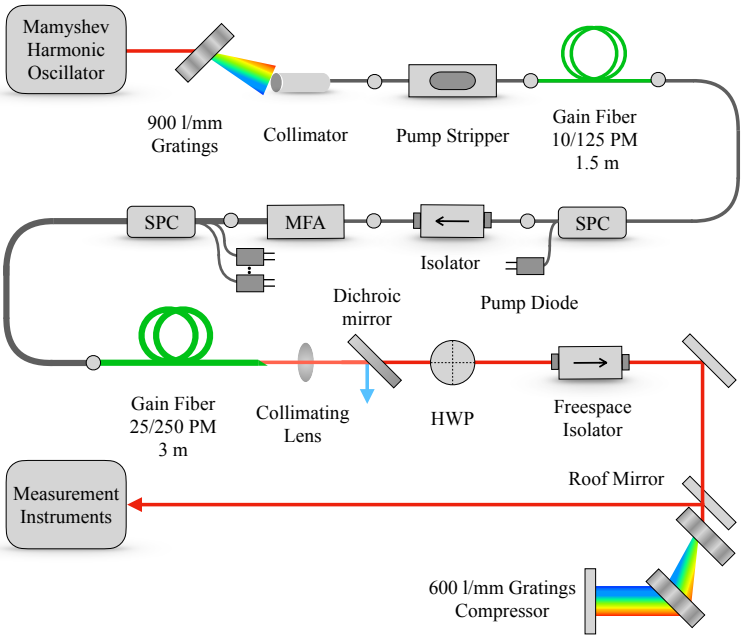

Figure 3.9: Schematic of the laser design. MFA: mode-field adaptor, SPC: signal pump combiner, HWP: half-wave plate.

the main amplifier. This pre-amplification stage was designed to have minimal nonlinear effects by keeping the fiber lengths short and controlling the pulse energy. The main amplifier had 3 m of 25/250 double-clad polarization maintaining gain fiber, designed in a forward pumping scheme. Optical pumping was done with laser diodes operating continuously at 976 nm.

The results of this system are shown in figure 3.10. By increasing the pump power in the amplifier, pulse energies increase, and pulses evolve beyond the similariton into the GMN regime. Around 300 nJ, Raman scattering becomes noticeable with a 30 dB lower maximum power than the highest signal spectral power.

This laser setup was mainly intended to implement a simple amplifier operating in the GMN regime. Due to its basic pre-amplifier design, changing the seed pulse parameters and utilizing the insight gained from the simulations was not practical as it required modifications in the pre-amplifier design. Since the primary intention of this thesis work was to design a burst mode amplifier in

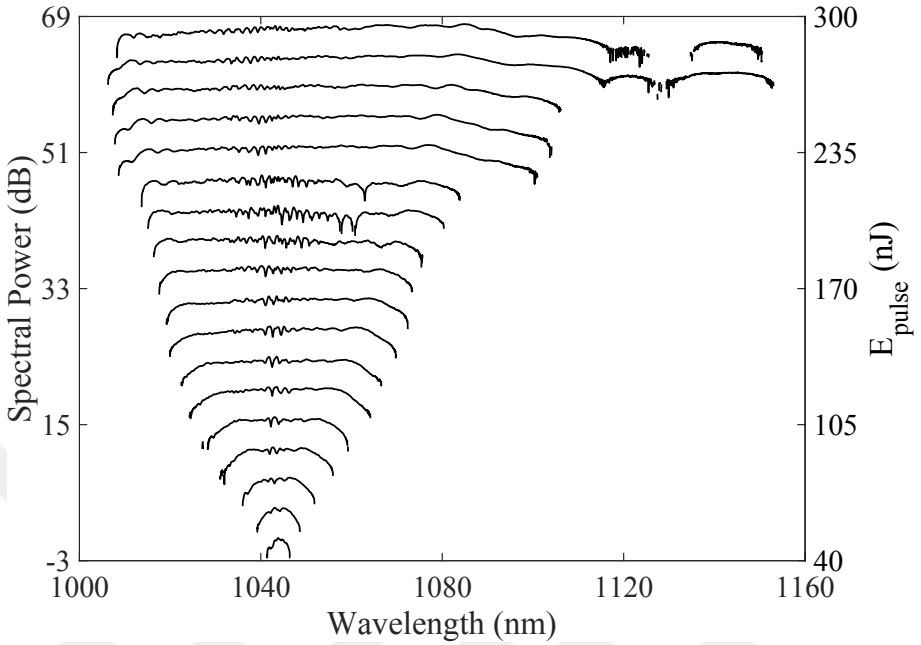

Figure 3.10: Experimental data show the spectral broadening due to increased pump power and, thus, increased pulse energy, where pulses evolve further into the GMN regime.

the GMN regime, in the next chapter, a more flexible laser design is presented operating in this regime and discussing certain aspects of its design.

Chapter 4

Ultrashort Pulse Bursts in Gain-Managed Nonlinearity Regime

In order to implement a GMN amplifier with signal bursts, the non-trivial impact of the burst-mode operation to gain dynamics and how this couples to the pulse evolution in the GMN must be understood. Before focusing on this, we begin with an overview of burst-mode operation.

Burst-mode amplifiers have several different forms whereby the signal, the pump, or both are pulsed. Signal-only bursts, where the gain medium is pumped continuously, are the most common form, as they afford reasonable flexibility on the number of pulses within a burst without the extra complications of pulsed pumping. Creating bursts through modulating the signal is typically accomplished by picking a group of pulses to define the burst using an optical gating device, such as an acousto-optic modulator. However, subsequent amplification is limited to high repetition rates. Otherwise, amplified spontaneous emission (ASE) can deplete the gain medium between the signal bursts. Typically, the burst repetition rate has to be at least 100 kHz, preferably close to 1 MHz, to avoid ASE generation.

The most versatile approach, which is also the most complicated, is to pulse-pump the gain medium, as well as seed the amplifier with bursts of signal pulses [6]. This requires the synchronization of the signal bursts and the pump pulses. In addition, the pump pulse can store energy for a finite duration before the arrival of the signal. Otherwise, ASE is still generated. Since the pumping duration is limited, energy storage becomes difficult, and the amplification efficiency is also significantly reduced. However, this is the only viable approach for high-energy bursts at low (kHz) repetition rates.

The final option is to modulate only the pump. Amplification occurs only when the gain medium has sufficient population inversion, thereby impressing a burst profile on the signal, but since the signal is not truly suppressed outside of the pump bursts, the extinction ratio is limited. Furthermore, since the gain dynamics cannot be modulated sufficiently fast, the minimum burst durations are long, in the microsecond or millisecond range. Therefore, despite its experimental simplicity, this method is not used only, but only as an addition to the use of signal-only bursts to generate what may be referred to as macrobursts, which are repeated at a much lower burst repetition rate.

Here, we consider only signal bursts formed by pulse picking using an acousto-optic modulator, which are amplified with a continuously pumped gain medium. Furthermore, we focus exclusively on attaining the GMN regime and do not discuss other aspects of burst-mode amplification.

4.1 GMN Regime with Pulse Bursts

In the laser design presented in the previous chapter, the simplicity of the pre-amplifier did not allow for the optimization of pulse evolution in the main amplifier. However, in the new design presented in this chapter, the pre-amplifier stage was improved to allow for increased degrees of freedom in shaping the seed pulse for the main amplifier. Additionally, the new design incorporates signal bursts, and in these lasers, to keep the seed parameters constant across different

burst duty cycles, a certain versatility in the pre-amplifier is needed; otherwise, seed pulses for different burst setups will have different characteristics resulting in unexpected evolution and compressed pulse duration. This chapter discusses the experimental laser design, the obtained results, and the amplification process with signal bursts and the GMN regime.

4.2 Experimental Results

Figure 4.1 shows the experimental setup. Pulses are generated in a passively and harmonically mode-locked NPE laser [43]. The recorded data in this work are at the fundamental repetition rate and its fourth harmonic corresponding to 60 and 240 MHz, respectively. The fiber output of the oscillator was first spliced to a stretch fiber to decrease the pulses' peak intensities and have linear amplification in the pre-amplifier. These pulses were picked by an acousto-optic modulator (AOM), creating signal bursts at various burst widths and repetition rates. After the pre-amplifier, a freespace segment was used to modify the seed pulse entering the main amplifier. In this freespace segment, adding various amounts of negative dispersion to the pulses using a grating compressor to de-chirp the stretched pulses and have a desired pulse duration was possible. Additionally, it was possible to spectrally filter the pulses using a beam-cutting mechanism placed after the grating compressor, changing their central wavelength and spectral width. After coupling the free space light back into the fiber line, using a mode-field adapter (MFA), a smooth transition was achieved going from single to multi-mode fibers. Next, the pump and signal lights were combined using a signal pump combiner (SPC), which was then spliced to the gain fiber. Fibers for MFA, SPC, and gain are all manufactured to have matching parameters, physical dimensions, and NAs to decrease the excitation of higher-order spatial modes at splice points.

The signal burst repetition rate, and the duty cycle values were chosen based on the theoretical and numerical insight gained in previous chapters, observing the deviations from theoretical expectations in the experimental results and commonly required burst parameters for burst-mode material processing applications.

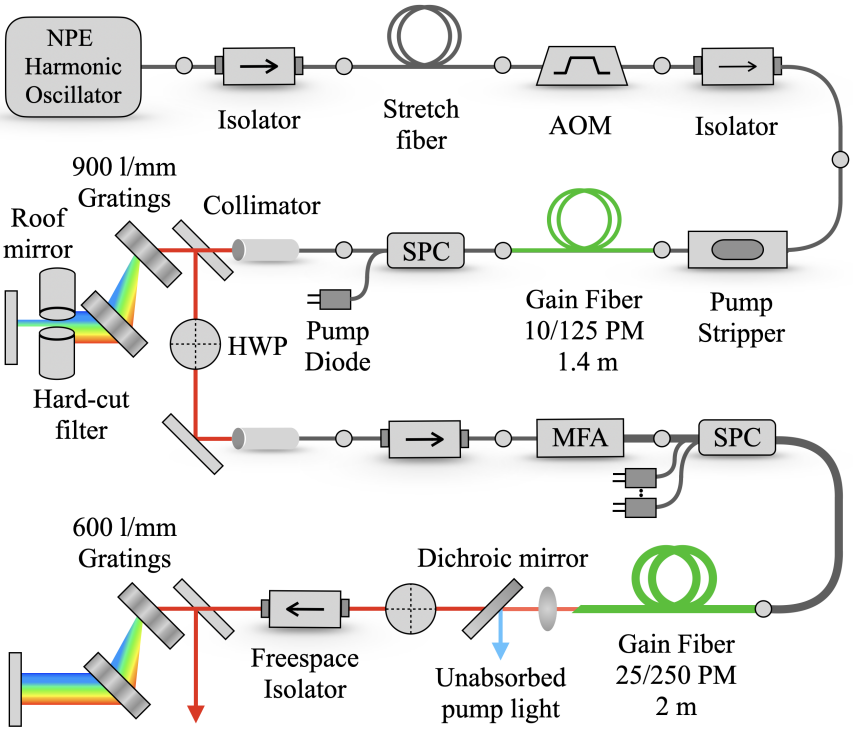

Figure 4.1: This figure shows the schematic of the laser system incorporating an acousto-optic modulator for burst creation. The laser consists of an oscillator, a pre-amplifier, a freespace section, and a final power amplifier.

For instance, a 1 MHz burst repetition rate corresponds to 1 µs separation between the bursts, which is much shorter than the calculated gain settling times discussed in the previous chapter for the power values used in our system. Under a specific burst duty cycle, the average signal power must be adjusted to reach the desired pulse energy. Alternatively, one can keep the average power constant and change the burst duty cycle to sweep over a range of pulse energies. The formulae relating burst and pulse energies are

$$E_{\text{burst}} = \frac{P_{\text{avg.}}}{f_{\text{burst}}}, \tag{4.1}$$

$$E_{\text{burst}} = \frac{T_{\text{burst, on}}}{T_{\text{pulse}}} E_{\text{pulse}} = T_{\text{burst, on}} f_{\text{pulse}} E_{\text{pulse}}. \tag{4.2}$$

Combining 4.1 and 4.2 we can write:

$$E_{\text{pulse}} = \frac{P_{\text{avg.}}}{f_{\text{burst}} T_{\text{burst, on}} f_{\text{pulse}}}. \tag{4.3}$$

Here, an important distinction must be made between $T_{\text{burst, on}}$ and T_{pulse}. Since bursts can have different duty cycles, when referring to burst duration, it is essential to specify whether it refers to the burst period or the on-time duration. To clarify, the "on" subscript was used in $T_{\text{burst, on}}$. Since the concept of duty cycle in ultrashort pulses is not of importance in our discussions, the expression T_{pulse} always refers to the period of the pulse train.

Table 4.1 shows the burst parameters used in our experiments. The pulse repetition rate was changeable with the harmonic oscillator, and according to that, burst on time was chosen to include from 5 up to 15 pulses.

Table 4.1: **Burst Parameters**

Parameter	Unit	Value
f_{pulse} (pulse repetition rate)	MHz	$\in \{60, 240\}$
$f_{\text{burst rep.}}$ (burst repetition rate)	MHz	1
T_{burst}	ns	$\in \{\frac{5}{\text{f}_{\text{pulse}}}, \cdots, \frac{15}{\text{f}_{\text{pulse}}}\}$

Therefore, to reach pulse energies ranging from tens up to hundreds of nanojoules at a pulse repetition rate of 240 MHz, the average signal power was kept constant, and the burst duty cycle was modified in each experiment. Table 4.2 shows these values in more detail.

Table 4.2: **Detailed Burst Parameters for $\mathbf{f_{pulse} = 240}$ MHz**

E_{pulse} (nJ)	f_{burst} (MHz)	$T_{\text{burst, on}}$ (ns)	$P_{\text{avg.}}$ (W)
393	1	58	5.5
423	1	54	5.5
⋮	⋮	⋮	⋮
785	1	30	5.5
917	1	25	5.5

Following the burst configurations in Table 4.2, after optimizing the seed parameters for the best GMN evolution, we obtained 47-fs-long pulses, inferred

from autocorrelation measurements, assuming a Gaussian pulse shape. The optical spectra in semi-log scale and the corresponding interferometric autocorrelation traces can be seen in Figure 4.2.

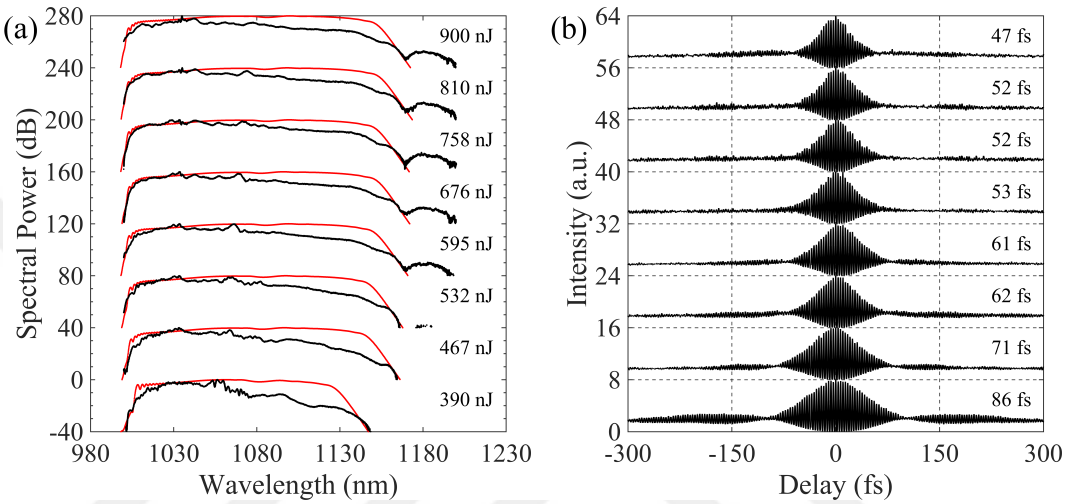

Figure 4.2: (a) Experimental (black) and numerical simulations (red) corresponding to constant average signal power and varying burst duty cycles resulting in higher pulse energies. (b) shows the corresponding interferometric autocorrelation traces and their Gaussian inferred pulse widths.

4.3 Effects of Gain Dynamics on Signal Bursts

There is an essential difference between non-burst and burst mode amplifiers. In traditional non-burst mode ones, for a given pump power, one would end up with a specific average signal power at the steady state, corresponding to a particular pulse energy. However, this is more complex in burst mode amplifiers since, for a variety of pump powers, the same pulse energy can still be obtained by changing the burst duty cycle. For instance, Table 4.3 shows different burst settings, resulting in a pulse energy of 600 nJ.

Table 4.3: **Detailed Burst Parameters for $\mathbf{f_{pulse} = 60}$ MHz**

E_{pulse} (nJ)	f_{burst} (MHz)	$T_{\text{burst, on}}$ (ns)	$P_{\text{avg.}}$ (W)
600	1	83	3
600	1	100	3.6
⋮	⋮	⋮	⋮
600	1	217	7.8
600	1	233	8.4

The ability to reach the same pulse energy under different pump powers and burst duty cycles would only be a technical detail if the final pulse in these different setups and experiments were the same, especially since the final pulse energies are the same. However, our further experimental results show noticeable differences in final pulses and spectra between the results of these experiments. Figure 4.3 shows that there are differences in both optical spectra and compressed pulses for different pump powers and burst duty cycles resulting in the same pulse energy. For instance, bursts with 233 ns on time, 1 MHz repetition rate and 8.4 W average signal power obtained Gaussian inferred pulse duration is 47 fs, but with 83 ns burst on time, 1 MHz repetition rate, and 3 W average signal power, 70 fs Gaussian inferred pulses were obtained, while in both cases pulse energy was 600 nJ. These differences are also noticeable in the shape of optical spectra.

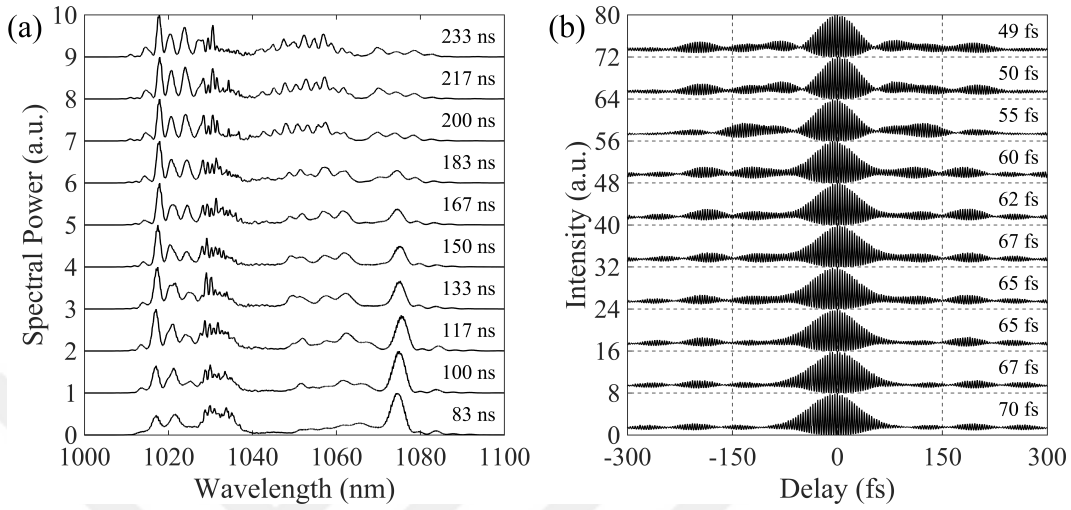

Figure 4.3: Despite obtaining the same pulse energy, the spectrum and the final compressed pulse duration differ for various pump powers and burst widths. (a) shows the spectra obtained for constant pulse energy at different burst on-times, with a constant 1 MHz burst repetition rate in all the cases, resulting in different burst duty cycles. (b) shows the corresponding interferometric autocorrelation and Gaussian inferred widths.

We assert that the primary source of this difference is due to pulses experiencing different gain profiles in each experiment. These different gain profiles come about due to the pump powers being different. Additionally, the GMN regime has its role to play. Namely, it has a very long spectrum surpassing the commonly used positive-gain regimes in Yb-doped fiber amplifiers. Thus, the amplification process in the GMN regime is highly dependent on the gain profile. The combination of (i) different pump and signal powers in different burst duty cycle experiments, resulting in slightly different gain profiles, and (ii) GMN regime's sensitivity to the gain spectrum, lead to such effects. For similariton pulses, on the other hand, these differences would be weaker since their spectra are only propagated in the positive gain spectral region, where the only difference is the amount of net gain, and the detailed shape of the gain spectrum is not modified. Figure 4.4 shows the same varying pump power and burst duty cycle experiments with pulses evolving to similariton and GMN regimes. The control between which regime to evolve was accomplished through controlling the amount of added chirp

to the pulses, subsequently changing their widths and peak powers. Figure 4.4 shows that similariton pulses are less sensitive to the changes in pump power and burst duty cycle. However, GMN pulses differ more in their spectra and final pulse durations.

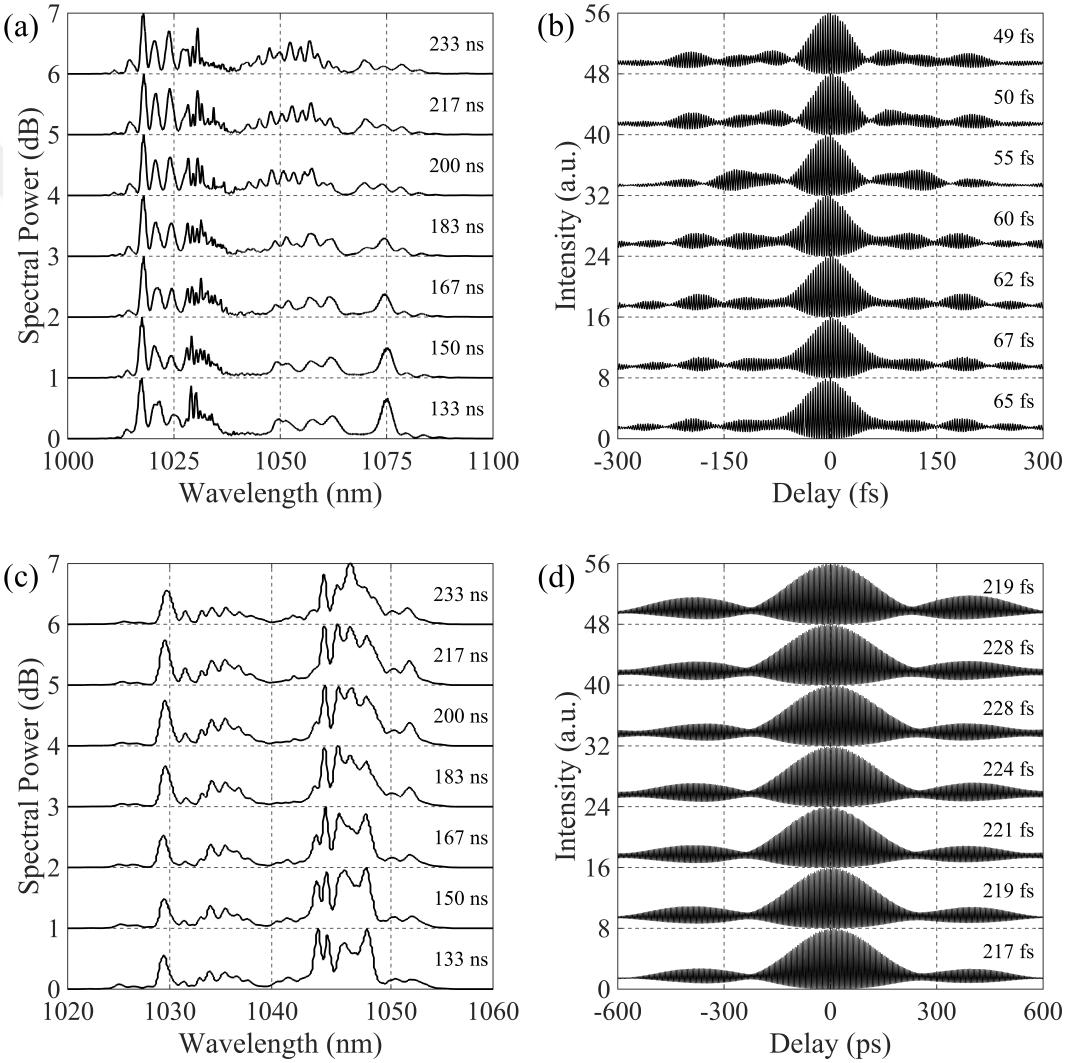

Figure 4.4: Due to having a more extended spectrum going beyond the positive gain regions, the GMN regime shows more sensitivity to the pump power and burst duty cycle changes compared to the similariton regime, which mainly evolves in the positive gain region.

In order to eliminate the possibility of other factors influencing the results,

the amplifier's stability was analyzed between different pump power and burst duty cycle experiments. Figure 4.5 (a) shows the settling of the optical spectrum for 15 minutes after the amplifier is turned on and set to operate in a specific power and burst duty cycle. The results show that the amplifier reaches spectral stability before 15 minutes. This is important because the spectrum, power, and autocorrelation measurements were always performed after the amplifier reached a steady state. Additionally, temperature measurements were taken using thermocouples attached to the outer coating of the gain fiber. Figure 4.5 (b) shows that between these experiments, the operation temperature did not differ more than 2° C. Comparing the circumference of the coating to the core, approximately between 20° or 40° C difference in the core is expected. These values are too small for any thermal-induced gain spectrum changes [27]. Additionally, as discussed in Chapter 2.3, if the burst's on-time average power becomes very high, the gain settling time during the burst becomes very short, or in other words, each pulse depletes a significant amount of energy from the gain medium, then pulses inside of a burst will experience unequal gains. This effect is a non-flat, exponential-like burst envelope after the amplification. To that end, to show that we do not have such effects in our setup, burst trains before and after amplification were measured and are shown for various burst lengths. Figure 4.5 (c) and (d) show these burst trains and their envelopes, measured before and after amplification, respectively.

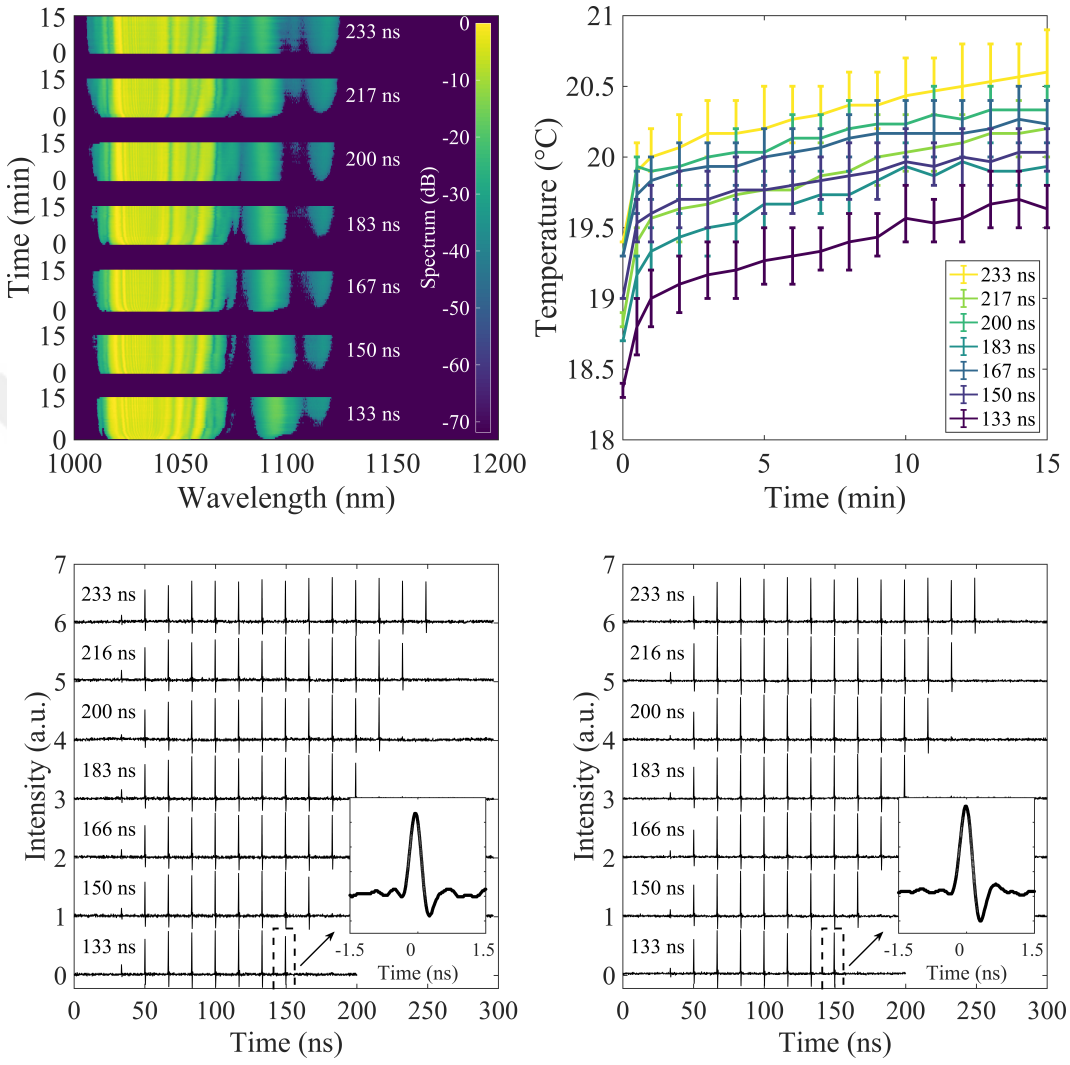

Figure 4.5: (a) Spectral evolution over time for each pump power and burst duty cycle experiment, recorded for 15 minutes. In all the cases, the spectrum settles before 15 minutes, and only the parts 40 and 50 dB weaker than the peak show some fluctuations. (b) Temperature data of the gain fiber measured from its outer coating at three different locations shows the differences are less than 2° C, hinting an approximately 20° to 40° C temperature difference in the core between the experiments. (c) and (d) show the burst profiles before and after amplification, respectively, measured with a non-saturated fast photodiode in the linear regime.

Since we have eliminated the potential sources that could cause the observed

spectral differences in different pump power and burst duty cycle experiments, an experimental measurement showing that gain profiles are different between these experiments could support our claims. As it is impossible to measure the powers midway in the fiber, only by looking at the signal and pump powers at the end of the fiber and having signal and pump spectra can we still numerically calculate the amount of gain at the end of the amplifier. The results of this analysis are presented in Figure 4.6. This shows that, indeed, between different pump power and burst duty cycle experiments, there are differences between the gain profiles.

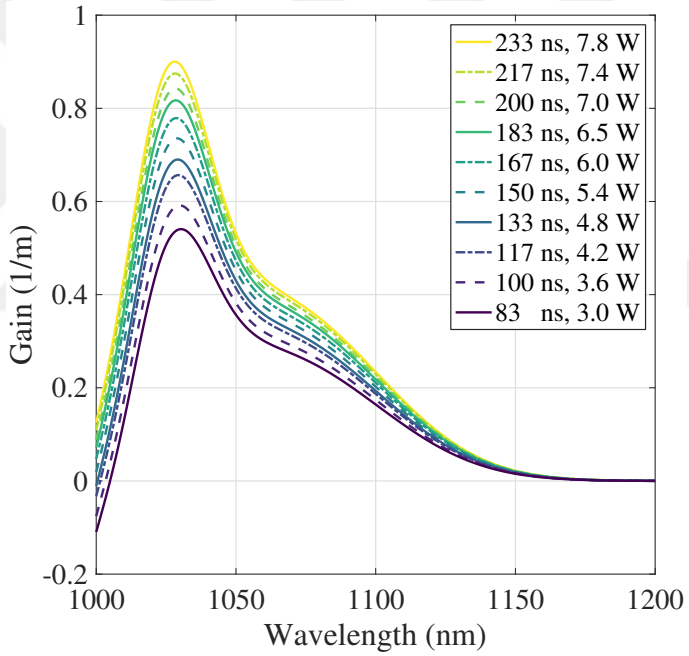

Figure 4.6: By measuring the signal and pump powers at the end of the gain fiber and signal and pump spectra and knowing the fiber parameters, the gain spectrum was numerically calculated at the end of the gain fiber. The results indicate that between varying pump power and burst duty cycle experiments, there are indeed differences in their gain profiles.

This trend is also noticeable in the macro parameters showing the performance of the gain medium. Table 4.4 shows the amplifier's pump-to-noise power conversion and pump absorption efficiency for these experiments. It can be seen that longer bursts with higher average powers have higher conversion efficiency,

hinting at differences in the underlying gain profiles.

Table 4.4: **Amplifier Parameters for Different Burst Duration**

T_{burst} (ns)	$P_{\text{signal}}/P_{\text{pump}}$ (%)	pump absorption (%)
83	46.90	91.92
100	49.34	92.16
117	50.73	92.18
133	52.22	92.48
150	53.55	92.55
167	54.15	92.66
183	54.36	92.72
200	55.61	92.73
217	55.70	92.96
233	55.94	92.97

Therefore, from these results, the amplification process in burst mode fiber lasers evolving towards the GMN regime shows a collective nature, in which the number of pulses inside the burst determines the type of evolution pulses will have.

Chapter 5

Conclusion and Future Work

This work first integrated a numerical model based on the nonlinear pulse propagation in optical fibers with a gain model that considers realistic gain cross-sections. With this, simulating the co-evolving gain spectrum in ultrafast fiber amplifiers was possible. The main advantage of this tool was being able to simulate the GMN regime, study some of its physical features, and design an amplifier operating in this regime. Further study of Yb doped gain fiber's response time allowed us to understand which power values in typical LMA gain fibers lead to slow gain effects where the amplification between pulses in a burst is equal. Combining these two, we were able to design a burst-mode amplifier operating in the GMN regime, reaching pulse energies around 1 µJ and 50 fs. Finally, the added degree of freedom from the burst mode laser allows us to reach the same pulse energy at different pump powers and burst duty cycles, as well as the sensitivity of the GMN regime to the profile of the gain spectrum, evolution, and the final features of the amplified pulses were different. Conceptually, the outstanding conclusion of this thesis is the emergence of non-trivial dependencies between the number and sequences of the pulses comprising the bursts and their amplification and nonlinear evolution in the GMN regime. In simple terms, the amplification process has apparent and non-negligible collective features. These effects surpass quantitative changes. If the dynamics are not carefully managed, the same pulse energies but different burst durations can entirely miss the GMN

regime, resulting in nearly an order of magnitude longer pulse durations. This collective nature is a clear break from the established paradigm for ultrafast pulse amplification, namely that the amplification can be understood by analyzing a single pulse. This simplification ceases to be correct in the burst-mode GMN regime.

The present thesis merely scratches the surface of these complex but rich collective dynamics. More progress is needed to thoroughly understand the full implication of the collective amplification characteristics. We conclude by briefly listing possible follow-up work toward a fuller understanding: It is necessary to develop the gain response time model to greater maturity to predict gain response in different burst-mode configurations. The basin of attraction of the GMN is not fully clarified. It should be explored further, particularly in relation to the parameters more relevant to burst-mode operation. The numerical model can be expanded to incorporate the gain dynamics more realistically. Finally, the collective nature of the pulse amplification should be explored in depth to identify the physical mechanisms at play more clearly, particularly the interplay of the Raman nonlinearities and the evolving gain profile across the amplifier in response to the transient gain dynamics triggered by the bursts.

Bibliography

[1] M. E. Fermann and I. Hartl, "Ultrafast fibre lasers," *Nature Photonics*, vol. 7, pp. 868–874, Nov. 2013.

[2] K.-H. Leitz, B. Redlingshöfer, Y. Reg, A. Otto, and M. Schmidt, "Metal Ablation with Short and Ultrashort Laser Pulses," *Physics Procedia*, vol. 12, pp. 230–238, Jan. 2011.

[3] B. Ali, I. V. Litvinyuk, and M. Rybachuk, "Femtosecond laser micromachining of diamond: Current research status, applications and challenges," *Carbon*, vol. 179, pp. 209–226, July 2021.

[4] C. Kerse, H. Kalaycıoğlu, P. Elahi, B. Çetin, D. K. Kesim, Ö. Akçaalan, S. Yavaş, M. D. Aşık, B. Öktem, H. Hoogland, R. Holzwarth, and F. Ö. Ilday, "Ablation-cooled material removal with ultrafast bursts of pulses," *Nature*, vol. 537, pp. 84–88, Sept. 2016.

[5] H. Kalaycioglu, K. Eken, and F. Ö. Ilday, "Fiber amplification of pulse bursts up to 20 μJpulse energy at 1 kHz repetition rate," *Optics Letters*, vol. 36, pp. 3383–3385, Sept. 2011.

[6] H. Kalaycıoğlu, Ö. Akçaalan, S. Yavaş, Y. B. Eldeniz, and F. Ö. Ilday, "Burst-mode Yb-doped fiber amplifier system optimized for low-repetition-rate operation," *JOSA B*, vol. 32, pp. 900–906, May 2015.

[7] P. Elahi, S. Yılmaz, Y. B. Eldeniz, and F. Ö. Ilday, "Generation of picosecond pulses directly from a 100 W, burst-mode, doping-managed Yb-doped fiber amplifier," *Optics Letters*, vol. 39, pp. 236–239, Jan. 2014.

[8] H. Kalaycıoğlu, Y. B. Eldeniz, Ö. Akçaalan, S. Yavaş, K. Gürel, M. Efe, and F. Ö. Ilday, "1 mJ pulse bursts from a Yb-doped fiber amplifier," *Optics Letters*, vol. 37, pp. 2586–2588, July 2012.

[9] H. Kalaycıoğlu, P. Elahi, Ö. Akçaalan, and F. Ö. Ilday, "High-Repetition-Rate Ultrafast Fiber Lasers for Material Processing," *IEEE Journal of Selected Topics in Quantum Electronics*, vol. 24, pp. 1–12, May 2018.

[10] S. Yavas, F. A. Uçak, İ. Ateşpare, M. Y. Kaya, S. G. Karamuk, G. Alpakut, and H. Kalaycioğlu, "High throughput ablation with ultrafast GHz burst fiber laser," in *Laser-Based Micro- and Nanoprocessing XV*, vol. 11674, pp. 223–228, SPIE, Mar. 2021.

[11] G. Bonamis, E. Audouard, C. Hönninger, J. Lopez, K. Mishchik, E. Mottay, and I. Manek-Hönninger, "Systematic study of laser ablation with GHz bursts of femtosecond pulses," *Optics Express*, vol. 28, pp. 27702–27714, Sept. 2020.

[12] H. Matsumoto, Z. Lin, J. N. Schrauben, and J. Kleinert, "Ultrafast laser ablation of silicon with ∼GHz bursts," *Journal of Laser Applications*, vol. 33, p. 032010, July 2021.

[13] H. Matsumoto, Z. Lin, and J. Kleinert, "Ultrafast laser ablation of copper with ˜GHz bursts," in *Laser Applications in Microelectronic and Optoelectronic Manufacturing (LAMOM) XXIII*, vol. 10519, p. 1051902, SPIE, Feb. 2018.

[14] K. Mishchik, G. Bonamis, J. Qiao, J. Lopez, E. Audouard, E. Mottay, C. Hönninger, and I. Manek-Hönninger, "High-efficiency femtosecond ablation of silicon with GHz repetition rate laser source," *Optics Letters*, vol. 44, pp. 2193–2196, May 2019.

[15] X. Wolters, G. Bonamis, K. Mishchick, E. Audouard, C. Hönninger, and E. Mottay, "High power GHz femtosecond laser for ablation efficiency increase," *Procedia Manufacturing*, vol. 36, pp. 200–207, Jan. 2019.

[16] R. W. Boyd, "Chapter 2 - Wave-Equation Description of Nonlinear Optical Interactions," in *Nonlinear Optics (Third Edition)* (R. W. Boyd, ed.), pp. 69–133, Burlington: Academic Press, Jan. 2008.

[17] R. W. Boyd, "Chapter 1 - The Nonlinear Optical Susceptibility," in *Nonlinear Optics (Third Edition)* (R. W. Boyd, ed.), pp. 1–67, Burlington: Academic Press, Jan. 2008.

[18] J. Dudley and S. Coen, "Numerical simulations and coherence properties of supercontinuum generation in photonic crystal and tapered optical fibers," *IEEE Journal of Selected Topics in Quantum Electronics*, vol. 8, pp. 651–659, May 2002.

[19] G. Agrawal, "Chapter 2 - Pulse Propagation in Fibers," in *Nonlinear Fiber Optics (Fifth Edition)* (G. Agrawal, ed.), Optics and Photonics, pp. 27–56, Boston: Academic Press, Jan. 2013.

[20] D. Hollenbeck and C. D. Cantrell, "Multiple-vibrational-mode model for fiber-optic Raman gain spectrum and response function," *JOSA B*, vol. 19, pp. 2886–2892, Dec. 2002.

[21] R. H. Stolen, J. P. Gordon, W. J. Tomlinson, and H. A. Haus, "Raman response function of silica-core fibers," *JOSA B*, vol. 6, pp. 1159–1166, June 1989.

[22] F. Ö. Ilday, J. Buckley, L. Kuznetsova, and F. W. Wise, "Generation of 36-femtosecond pulses from a ytterbium fiber laser," *Optics Express*, vol. 11, pp. 3550–3554, Dec. 2003.

[23] L. DeLoach, S. Payne, L. Chase, L. Smith, W. Kway, and W. Krupke, "Evaluation of absorption and emission properties of Yb/sup 3+/ doped crystals for laser applications," *IEEE Journal of Quantum Electronics*, vol. 29, pp. 1179–1191, Apr. 1993.

[24] W. Krupke, "Ytterbium solid-state lasers. The first decade," *IEEE Journal of Selected Topics in Quantum Electronics*, vol. 6, pp. 1287–1296, Nov. 2000.

[25] R. Paschotta, J. Nilsson, A. Tropper, and D. Hanna, "Ytterbium-doped fiber amplifiers," *IEEE Journal of Quantum Electronics*, vol. 33, pp. 1049–1056, July 1997.

[26] S. Unger, A. Schwuchow, S. Jetschke, V. Reichel, M. Leich, A. Scheffel, and J. Kirchhof, "Influence of aluminum-phosphorus codoping on optical properties of ytterbium-doped laser fibers," in *Optical Components and Materials VI*, vol. 7212, pp. 324–332, SPIE, Feb. 2009.

[27] T. Newell, P. Peterson, A. Gavrielides, and M. Sharma, "Temperature Effects on the Emission Properties of Yb-Doped Fiber (Postprint)," Nov. 2006.

[28] Durairaj, Vasuki, *https://aaltodoc.aalto.fi/handle/123456789/10447*. Ms Thesis, Alto University, Finland, June 2013.

[29] Şenel, Çağrı, *Numerical Modeling, Design, and Time-Frequency Metrology Applications of Low-Noise Optical Frequency Combs*. PhD thesis, Boğaziçi Unıversıty, Turkey, 2022.

[30] J. Hult, "A Fourth-Order Runge–Kutta in the Interaction Picture Method for Simulating Supercontinuum Generation in Optical Fibers," *Journal of Lightwave Technology*, vol. 25, pp. 3770–3775, Dec. 2007.

[31] M. E. Fermann, V. I. Kruglov, B. C. Thomsen, J. M. Dudley, and J. D. Harvey, "Self-Similar Propagation and Amplification of Parabolic Pulses in Optical Fibers," *Physical Review Letters*, vol. 84, pp. 6010–6013, June 2000.

[32] P. Sidorenko, W. Fu, and F. Wise, "Nonlinear ultrafast fiber amplifiers beyond the gain-narrowing limit," *Optica*, vol. 6, pp. 1328–1333, Oct. 2019.

[33] S. Wang, B. Liu, M. Hu, and C. Wang, "On the Efficiency of Parabolic Self-Similar Pulse Evolution in Fiber Amplifiers with Gain Shaping," *Journal of Lightwave Technology*, vol. 34, pp. 3023–3034, July 2016.

[34] M. E. Fermann and I. Hartl, "Ultrafast Fiber Laser Technology," *IEEE Journal of Selected Topics in Quantum Electronics*, vol. 15, pp. 191–206, Jan. 2009.

[35] F. Ö. Ilday, J. R. Buckley, W. G. Clark, and F. W. Wise, "Self-Similar Evolution of Parabolic Pulses in a Laser," *Physical Review Letters*, vol. 92, p. 213902, May 2004.

[36] A. C. Peacock, R. J. Kruhlak, J. D. Harvey, and J. M. Dudley, "Solitary pulse propagation in high gain optical fiber amplifiers with normal group velocity dispersion," *Optics Communications*, vol. 206, pp. 171–177, May 2002.

[37] D. B. Soh, J. Nilsson, and A. B. Grudinin, "Efficient femtosecond pulse generation using a parabolic amplifier combined with a pulse compressor. II. Finite gain-bandwidth effect," *JOSA B*, vol. 23, pp. 10–19, Jan. 2006.

[38] P. Repgen, D. Wandt, U. Morgner, J. Neumann, and D. Kracht, "Sub-50 fs, µJ-level pulses from a Mamyshev oscillator–amplifier system," *Optics Letters*, vol. 44, pp. 5973–5976, Dec. 2019.

[39] P. Sidorenko and F. Wise, "Generation of 1 µJ and 40 fs pulses from a large mode area gain-managed nonlinear amplifier," *Optics Letters*, vol. 45, pp. 4084–4087, July 2020.

[40] D. Tomaszewska-Rolla, R. Lindberg, V. Pasiskevicius, F. Laurell, and G. Soboń, "A comparative study of an Yb-doped fiber gain-managed nonlinear amplifier seeded by femtosecond fiber lasers," *Scientific Reports*, vol. 12, p. 404, Jan. 2022.

[41] L. Zheng, A. Kausas, and T. Taira, ">MW peak power at 266 nm, low jitter kHz repetition rate from intense pumped microlaser," *Optics Express*, vol. 24, pp. 28748–28760, Dec. 2016.

[42] Y. Wang, S. Y. Set, and S. Yamashita, "Active mode-locking via pump modulation in a Tm-doped fiber laser," *APL Photonics*, vol. 1, p. 071303, Oct. 2016.

[43] M. Laçin, P. Repgen, A. Şura, Ç. Şenel, and F. Ö. Ilday, "Analogy of harmonic modelocked pulses to trapped Brownian particles improves laser performance," *Applied Physics B*, vol. 129, p. 46, Feb. 2023.